Master's thesis

NTNU
Norwegian University of Science and Technology
Faculty of Engineering
Department of Marine Technology

Erlend Mørch Grova

Actuation of loads by using fans, and application to hydrodynamic testing

Master's thesis in Marine Technology
Supervisor: Thomas Sauder
June 2023

NTNU
Norwegian University of
Science and Technology

Erlend Mørch Grova

Actuation of loads by using fans, and application to hydrodynamic testing

Master's thesis in Marine Technology
Supervisor: Thomas Sauder
June 2023

Norwegian University of Science and Technology
Faculty of Engineering
Department of Marine Technology

NTNU
Norwegian University of
Science and Technology

NTNU Trondheim
Norwegian University of Science and Technology
Department of Marine Technology

MASTER OF TECHNOLOGY THESIS DEFINITION (30 SP)

Name of the candidate: Grova, Erlend Mørch
Field of study: Marine Cybernetics
Thesis title (English): Actuation of loads by using fans, and application to hydrodynamic testing

Background

The dynamic behaviour of floating wind turbines (FWT) is complex, as the FWT is strongly affected by both hydrodynamic and aerodynamic loads. In this context, small-scale experimental testing can be very beneficial to improve the accuracy of the numerical simulations. However, the challenge with model testing is that the hydrodynamic and aerodynamic forces scale differently. These issues can be mitigated by using a cyber-physical (hybrid) solution where the aerodynamic loads are computed, and applied on the structure by automatically controlled actuators, while wave and current loads are physical.

Various types of actuators are currently in use: fans, winches, cable-driven robots (composed of several winches), hexacopters, etc… This study will focus on applying the aerodynamic loads with fans.

The objective is to design, and build an experimental setup aimed at assessing the accuracy of a multi-fan-based actuation method to apply several load components. A particular focus will be given to jet interaction.

Scope of work

1. Perform a background and literature review on the application of wind loads in model testing, with particular focus on floating wind turbines.
2. For fan-based solutions, outline typical specifications of relevant fans (thrust, weight, …), and review existing literature on interaction between several fans, and allocation methods.
3. Design an experiment enabling to assess the performance of a selected fan system. Several load components should be monitored, and the interaction between several fans should be investigated.
4. Build the experimental apparatus to measure the actual applied load. This includes instrumentation, mechanical work and mechatronics.
5. Define a series of tests aiming at validating the experimental setup itself, and then at assessing the multi-fan-based actuation method. Perform tests in the lab.
6. Present the work performed in the project thesis in a structured manner, and conclude on the achievements, lessons learned, and possible improvements.

Execution of the work

The student shall at startup provide a week plan of work for the project period, with main activities and milestones.

Every week throughout the project period, the candidate shall send a status email to the supervisor and co-advisors, providing two brief bulleted lists: 1) work done during the recent week, and 2) work planned to be done next week. The student should flag needs for additional meetings with his/her supervisor, others than those already planned.

The scope of work may prove different from initially anticipated. By the approval from the supervisor, described topics may be deleted or reduced in extent without consequences with regard to grading.

The candidate shall present personal contribution to the resolution of problems within the scope of work. Theories and conclusions should be based on mathematical derivations and logic reasoning identifying the various steps in the deduction.

The project will be performed in collaboration with 7Waves (https://www.7waves.no/) which will contribute to design and cover the costs for rig, actuators and controllers. NTNU will provide the required instrumentation to measure the loads.

Project report

The report shall be organized in a logical structure to give a clear exposition of background, problem, design, results, and critical analysis. The text should be brief and to the point, with a clear language. Rigorous mathematical deductions and illustrating figures are preferred over lengthy textual descriptions. It shall be written in English and contain the following elements: title page, abstract, project definition, list of symbols and acronyms, table of contents, introduction (project background/motivation, objectives, scope and delimitations, and contributions), technical background and literature review, problem formulation, method, results and analysis, conclusions with recommendations for further work, references, and optional appendices. Figures, tables, and equations shall be numerated. LaTeX typesetting is preferred.

The original contribution of the candidate and material taken from other sources shall be clearly identified. Work from other sources shall be properly acknowledged using quotations and a Harvard citation style (e.g. natbib Latex package). The work is expected to be conducted in an honest and ethical manner, without any sort of plagiarism and misconduct.

NTNU can use the results freely in research and teaching by proper referencing, unless otherwise agreed upon. 7Waves can freely use the results of the research.

The report shall be submitted with an electronic copy to the main supervisor and department according to NTNU administrative procedures. The final revised version of this project definition shall be included after the title page. Computer code, pictures, videos, dataseries, etc., shall be included electronically with the report.

Start date: August 31st , 2022

Due date - fall project: December 16th 2022

Due date - MSc thesis: June 2023

Supervisor: Thomas Sauder

Digitally signed
by Sauder
Thomas Michel
Date: 2023.06.07
15:17:12 +02'00'

Abstract

This thesis aimed at designing, building, and testing an experimental setup using a multi-fan-based actuation method to apply several load components. The objective was to check the feasibility of applying the aerodynamic loads on an International Energy Agency (IEA) 15-megawatt (MW) floating wind turbine (FWT) with fans for cyber-physical testing.

The final solution consisted of a steel base and beam, a 3D-printed connection hub, configurable fan arms with actuators, a power supply, controllers, a load cell, and an accelerometer. The fan-based solution was able to induce loads in different configurations concerning the number of fans and their orientation. Multiple static tests were performed, and the results showed that the different fan arms were interchangeable and induced similar loads, with minor variations due to error sources in the setup. However, due to the bending of the fan arms when inducing forces, the resulting loads would be inaccurate, even if the results were repeatable. Furthermore, an interaction effect was shown, dependent on the distance between configured fan arms and the fans' revolutions per second (rps), which could decrease the results' precision and accuracy.

The solution would not be suitable for dynamic testing. The inaccuracies in the results were too significant for the setup to be able to follow a dynamic signal correctly, and the acceleration and velocity of the fans would also need to be increased. Design changes and improvements would have to be made to use the solution for cyber-physical testing.

Sammendrag

Denne masteroppgaven hadde som mål å designe, bygge og teste et eksperimentelt oppsett ved hjelp av en viftebasert belastningsmetode for å påføre flere laster. Målet var å se på muligheten for å påføre aerodynamiske laster på en IEA 15 MW flytende vindturbin ved hjelp av vifter for hybrid testing.

Løsningen besto av en stålbase og -bjelke, en 3D-printet kule, konfigurerbare viftearmer, en strømforsyning, kontrollere, en lastcelle og et akselerometer. Vifteløsningen kunne påføre belastninger i ulike konfigurasjoner med hensyn til både antall vifter og deres orientering. Flere statiske tester ble utført, og resultatene viste at de forskjellige viftearmene var utskiftbare og induserte lignende belastninger, med mindre variasjoner på grunn av feilkilder i oppsettet. Resultatene var repeterbare, men de resulterende lastene var unøyaktige på grunn av bøyning av viftearmene når de påførte krefter. Videre ble det vist en interaksjonseffekt som var avhengig av avstanden mellom viftearmene og deres rps, noe som kunne medføre reduksjon i presisjonen og nøyaktigheten til resultatene.

Løsningen vil ikke være egnet for dynamisk testing. Unøyaktighetene i resultatene var for betydelige for at oppsettet kunne følge et dynamisk signal riktig, og akselerasjonen og hastigheten til viftene vil også måtte økes. Designendringer og forbedringer vil måtte gjennomføres for å kunne bruke løsningen til hybrid testing.

Acknowledgements

First and foremost, I would like to extend my deepest gratitude to my supervisor, Thomas Sauder, for his invaluable guidance, expertise, and support throughout this master's thesis. His feedback and knowledge have been instrumental in completing this academic work. I could not have accomplished this without his help.

I would also like to extend my gratitude to 7Waves. Their collaboration and resources have been indispensable in conducting the necessary experiments for this thesis.

Furthermore, I would like to acknowledge the contributions of Robert Opland, who have helped me tremendously with the design, the measurements, and my numerous questions. He has been integral to the completion of the master's thesis.

I am grateful to Trond Insett for his assistance with the design of the solution, the 3D printing, and his willingness to help throughout all steps of the process. His contributions have been crucial for the creation of the experimental setup.

Moreover, I would like to express my appreciation to Ole Erik Vinje for his support in handling mechanical components, construction, and welding. The setup could not have been built without him.

I am thankful to Øyvind Berg Magnussen and Fredrik Brun Larsen for sharing their expertise and providing help with the implementation and utilization of Odrive, the controller and actuator used in the thesis.

Thanks should also go to Carlos Eduardo Silva de Souza, SINTEF Ocean, for providing time series for the IEA 15 MW wind turbine.

Lastly, I would like to acknowledge friends, family, and colleagues who have consistently supported and encouraged me during my time at the Norwegian University of Science and Technology (NTNU). Thank you.

Contents

List of Figures

List of Tables

List of Abbreviations

CDPR	**C**able **D**riven **P**arallel **R**obot
DOF	**D**egrees **O**f **F**reedom
FWT	**F**loating **W**ind **T**urbine
GUI	**G**raphical **U**ser **I**nterface
IEA	**I**nternatonal **E**nergy **A**gency
MW	**M**egawatt
NTNU	**N**orwegian **U**niversity of **S**cience and **T**echnology
rpm	**r**evoutions **p**er **m**inute
rps	**r**evoutions **p**er **s**econd
TLP	**T**ension **L**eg **P**latform

Chapter 1

Introduction

The content of Chapters 1, 2, 3, and 4 were reproduced/adapted from the authors' project report [1].

The dynamic behavior of a floating wind turbine is complex, as the FWT is strongly affected by both hydrodynamic and aerodynamic loads. In this context, small-scale experimental testing can be very beneficial in improving the accuracy of numerical simulations. However, the challenge with model testing is that the hydrodynamic and aerodynamic forces scale differently. These issues can be mitigated using a cyber-physical (hybrid) solution where the aerodynamic loads are computed and applied to the structure by automatically controlled actuators, while wave and current loads are physical. Various actuators are currently in use: fans, a winch, cable-driven robots (composed of several winches), hexacopters, etc. This thesis focused on designing and building a solution using fans. The solution aimed at assessing the accuracy of a multi-fan-based actuation method to apply several load components, with a particular focus on jet interaction.

Chapter 2

Background

2.1 Cyber-physical testing

Cyber-physical testing is the combination of experiments and simulations run in real-time using a control system. The experiments are the physical substructure, while the simulations function as the numerical substructure of the tests. Hybrid testing solves problems that cannot be accurately solved using purely numerical models or physical experiments. This could, for example, be due to inadequate testing infrastructure, incompatibility regarding scaling, or increased efficiency by doing component testing [2].

Hybrid testing is based on flow control or effort control. Flow control is about controlling the kinematics of the system, and the balance of flow between the numerical and physical substructures is known as compatibility. Effort control is about controlling the loads on the system, and the balance of effort is known as equilibrium [3]. The type of control chosen varies depending on the properties of the physical substructures. Effort control has so far been used for the hybrid testing of marine systems.

2.1.1 History

Cyber-physical testing was first utilized in 1975 for buildings and infrastructure by Takanashi et al. [4] [5] Since then, hybrid testing has been used for several industries, such as aerospace, electrical, and marine engineering. It has also been utilized for fields of engineering, such as for engine testing [6], chassis dynamics [7] and thermomechanics [8] [5].

2.1.2 Types of methods

For cyber-physical testing, multiple methods have been used to apply the loads generated by the numerical substructure. Some experiments demanded a specific type of control due to the dynamics of the experiment. Hydrodynamic testing could not

be performed at low speed due to the changes in restoring and damping forces for different velocities.

One method used for hybrid testing has been hydraulic actuators, which have been used for seismic testing by utilizing flow control [9]. For marine hydrodynamics, some methods of cyber-physical testing included Cable-Driven Parallel Robots (CDPR) [10], ducted fans [11] or multi-fans [12].

2.1.2.1 Cable-Driven Parallel Robots

Cable-Driven Parallel Robots have been a way to apply load to the physical substructure computed by the numerical substructure. This method was based on setting up winches that imposed a load or moment on the physical substructure. CDPR controlled the cables' tension to apply the desired load on the model [13]. A setup of Cable-Driven Parallel Robots can be seen in Figure 2.1.

FIGURE 2.1: Setup of CDPR - from [10]

The Cable-Driven Parallel Robots had certain constraints that needed to be satisfied. Firstly, the cables should not become slack. This would lead to a loss of controllability and would cause snatch loads when tension was regained. In addition, the tension in the cables should not exceed a specified safety value, as this would cause fatigue and, ultimately, failure of the cables. Furthermore, the applied loads on the model should be applied correctly even with motions of the physical substructure [13].

The CDPR method has been used at SINTEF Ocean for real-time hybrid model testing on floating wind turbines. This method was found to work well with a high level of repeatability by Thys et al. [14] when tested for a 10-MW semisubmersible floating wind turbine. A CDPR setup performed at SINTEF Ocean can be seen in Figure 2.2 [15]:

FIGURE 2.2: Setup of CDPR in a wave basin - from [15]

The CDPR method has also been used at SINTEF Ocean for free-running hydrodynamic tests of a wind-assisted cargo ship [16]. This study applied the computed wind loads on the ship by CDPR and documented that the resulting loads were emulated with high precision and repeatability.

2.1.2.2 Fans

Another frequently used method for cyber-physical testing for marine hydrodynamics was fans. Multiple studies have used fan solutions, such as Azcona et al. [11] utilizing a ducted fan or Battistella et al. [12] using multi-fans. The fans were used to apply loads on the physical substructure and could be set up in different configurations to model multiple degrees of freedom (DOF). Depending on the setup, the fans could cover up to six components and were also based on effort control. An example of a ducted fan setup can be seen in Figure 2.3:

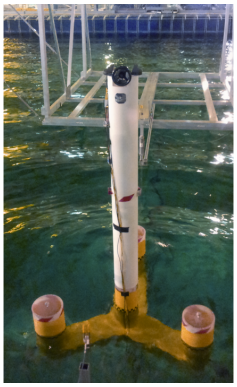

FIGURE 2.3: Setup with ducted fan - from [11]

2.1.2.3 Other methods

Another method used for cyber-physical testing of floating wind turbines has been to perform hybrid testing in a wind tunnel. This was done at Politecnico di Milano using a custom-made hydraulic actuation system, where the floater motions were numerically simulated [17]. This method has been used by Bayati et al. [18], which concluded that the results were similar to numerical methods for the platform dynamics [19].

A hexapod solution has been used at École Centrale de Nantes by Arnal et al. [20] to benchmark a fan-based solution. This study showed that the system could closely match the numerical high-frequency aerodynamic loads. A setup with a parallel kinematic machine in the wind tunnel at Politecnico di Milano can be seen in Figure 2.4:

FIGURE 2.4: Setup with a parallel kinematic machine in the wind tunnel at Politecnico di Milano - from [21]

Another method used to induce loads for hybrid testing has been robotic arms.

2.1.3 The fan solutions

As mentioned previously, the fan solutions included single ducted fan solutions and different combinations of multi-fan solutions. The multi-fan solutions could achieve varying degrees of freedom depending on the number of rotors and the orientation of the fans. This literature study has mainly focused on fan solutions concerning floating wind turbines.

2.1.3.1 Ducted fans

Ducted fans have been used in multiple cyber-physical tests of floating wind turbines. The setup used by Azcona et al. [11], seen in Figure 2.3, consisted of a single ducted fan on a modeled semisubmersible 6 MW floating wind turbine. Only the aerodynamic thrust was reproduced by the fan for this study, and the results showed that it was able to closely match the numerical results for the surge and pitch motions.

A different ducted fan setup was used with a modeled 5 MW tension leg platform (TLP) wind turbine by Wright et al. [22] This study used the fan as a steady thrust force and compared the dynamic response of the model with and without a spring damper. The ducted fan in this study was also only tested for loads in one degree of freedom.

2.1.3.2 Multi-fans

Multi-fan setups have also been utilized for cyber-physical testing. Batistella et al. [12] created a multi-fan that could change the number, size, and orientation of its rotors. The maximum amount of rotors used was 6, and the setup can be seen in Figure 2.5. The setup generated both the thrust force and the aerodynamic moments due to the changeability of its rotors. The study focused on how effective the multi-fan system was at emulating the thrust force, and the results showed that it was able to generate 87 % of the numerically calculated aerodynamic loads [12].

FIGURE 2.5: Multi-fan setup with 6 rotors - from [12]

Vittori et al. [23] used a multi-propeller actuator of four propellers to generate pitch and yaw moments in addition to the thrust force. The test setup can be seen in Figure 2.6. The study compared the experimental motions of the model with a numerical model in OpenFAST and found the responses to match well for both surge, pitch, and yaw.

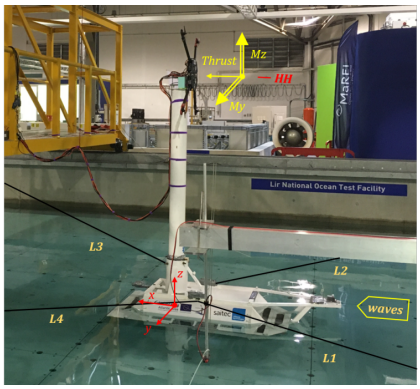

FIGURE 2.6: Multi-fan setup with 4 rotors - from [23]

The same multi-propeller actuator was also used by Hmedi et al. [24] to test the operational performance of a TLP with a 10 MW wind turbine. The study performed tests that included free decays, regular waves, steady wind, regular waves with steady wind, irregular waves and turbulent wind, 50-year extreme condition, and emergency shutdown. The study's results found the system to be replicated with high accuracy during the testing.

A ducted fan setup of two separate fans has also been studied [25], as shown in Figure 2.7. The study tested how the experimental precision changes for a physical wave basin test by introducing a steady thrust force and gyroscopic loads. The results showed a significant reduction of precision with the added thruster load, but not a large impact with the gyroscopic loads.

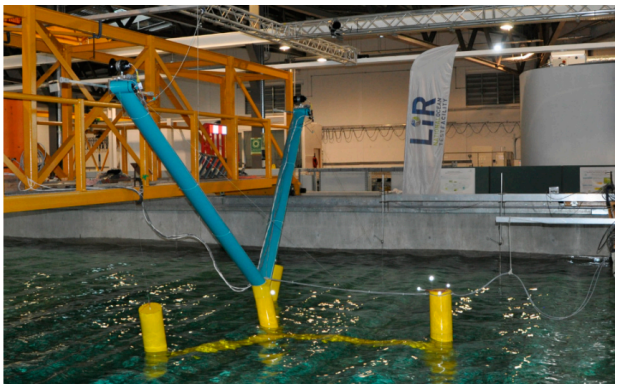

FIGURE 2.7: Setup with two ducted fans - from [25]

A different Multi-Propeller Device was created and used by Otter et al. [26] This design consisted of 6 propellers with different orientations, as shown in Figure 2.8. This study compared the experimental results of the model to numerical simulations from FAST v8 and compared rotor thrust, rotor torque, and yaw moment. The setup performed well for rotor thrust and torque, but not for the yaw moment.

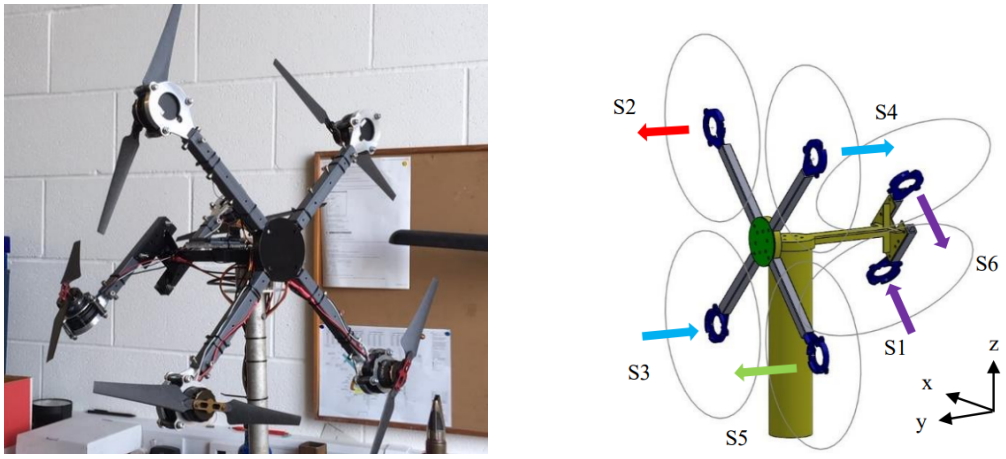

FIGURE 2.8: Multi-fan setup with 6 rotors - from [26]

2.1.4 Summary

Cyber-physical testing could utilize multiple methods to solve problems that could not be accurately solved using purely physical or numerical models. In marine hydrodynamics, the methods mostly used effort control and were chosen based on the properties of the physical substructure. For floating wind turbines, these methods included CDPR and different fan solutions. Existing multi-fan-based solutions gave promising results, but some challenges were still related to the simultaneous application of multiple load components.

Chapter 3

Functional requirements

This master's thesis aimed at assessing the accuracy of a multi-fan-based actuation method to apply aerodynamic loads for cyber-physical testing. A solution was built to achieve this, which needed to satisfy functional requirements based on the performed literature study. The requirements were divided into mechanical requirements, documentation tests, and a test matrix. The tests were then performed with static loads.

3.1 Mechanical requirements

Parameters chosen for the fan solution were kept equal to SINTEF Ocean's CDPR solution to have the option to compare the results. The scaling law was then chosen as Froude scaling and was set to $\lambda = \frac{1}{42.5}$, as used for the CDPR solution. Furthermore, the magnitude of loads was chosen based on time series of six DOF wind loads for an IEA 15 MW floating wind turbine [27]. In addition, the mechanical solution needed the ability to induce and measure loads in all six degrees of freedom. Formulas for Froude scaling of time t, force F, and moment M from real size to model size were sourced from [5] and can be seen as:

$$t_F = \sqrt{\lambda} \cdot t_M \tag{3.1}$$

$$F_F = \frac{\rho_F}{\rho_M} \cdot \lambda^3 F_M \tag{3.2}$$

$$M_F = \frac{\rho_F}{\rho_M} \cdot \lambda^4 M_M \tag{3.3}$$

Here, $\frac{\rho_F}{\rho_M}$ was the relative water density between actual size and model size. With the given wind loads, $\lambda = \frac{1}{42.5}$ and using formula 3.2 and 3.3, the necessary forces were calculated to be in the range of up to 40 N, and the moments about rotor center

were up to 15 Nm. The total mass of the IEA 15 MW floating wind turbine was 1 017 000 kg, which gave a maximum mass limit for the fan solution using the formula 3.2 of 13.2 kg for dynamic tests. The forces and moments induced on the model were to be captured by a 6-component load cell and a 3-axis accelerometer. This meant a signal amplifier with at least nine sensor inputs was also needed.

The accuracy chosen for this thesis was 0.2 N, as this was the standard benchmark used in other similar studies, such as in [28] and [29]. The sampling frequency has varied a lot for the different studies. For example, Azcona et al. [11] used a sampling frequency of 120 Hz, while Sauder et al. [2] used a frequency of 600 Hz for angular velocities and 100 Hz for position and attitude. A sampling frequency of 200 Hz was chosen for this setup after discussions with Robert Opland, Senior Engineer at NTNU, as this was satisfactory for the accuracy of the measurements. A clearance from the ground of at least 0.25 m was needed to reduce the uncertainty in the results that would arise from flow disturbance due to proximity to a surface [30]. With an added safety margin, this was set to be at least 0.4 m. Due to the maximum moment requirements for the study of 15 Nm, and the minimum clearance from the surface, a fan arm with a length of a minimum of 0.5 m was needed. In addition, the solution needed the ability to induce the wind loads in all 6 degrees of freedom for different fan arm configurations. The setup, therefore, needed multiple attachment points to accommodate this. Moreover, the fan arms needed the ability to connect to and disconnect from the hub to change the configurations.

The summarized mechanical requirements for the model can be seen in Table 3.1:

TABLE 3.1: Mechanical requirements

Mechanical characteristics	**Value**
Floating Wind Turbine	IEA 15 MW
DOF	6
Accuracy	0.2 N
Maximum Force	40 N
Maximum Moment	15 Nm
Mass limit	13.2 kg
λ	$\frac{1}{42.5}$
Sampling frequency	200 Hz
Minimum clearance from surface	0.4 m
Minimum fan arm length	0.5 m

3.2 Functional tests

Different tests were required to validate the system and measure its performance. These tests included both documentation and performance tests.

3.2.1 Documentation tests

Specific documentation tests had to be performed to see if the mechanical solution worked as intended. For these verification tests, it was important that the components worked as intended and still functioned when combined into the complete mechanical setup. If the solution performed as expected, future errors would be easier to debug.

These tests included verification of:

- The setup and the instrumentation
- The software
- The test repeatability
- The fan arm performance
- The eigenfrequencies

3.2.2 Test matrix

Different setups were examined to test the fan solution's capabilities. Each test was performed with a static load, and the results were then used to provide insight into the fan solution's performance. Different combinations of loads and configurations were tested to research the limitations of the setup and its use cases. A particular focus was placed on jet interaction.

The tests were summarized in a test matrix as:

TABLE 3.2: Test matrix

Test number	**Description**	**Number of fans**
1	Static force test with multiple fan arms in parallel configuration	2
2	Static force test with multiple fan arms in opposite configuration	2
3	Interaction test, varying angle of static rotor	2
4	Interaction test, varying rps	2
5	Interaction test, varying angle of dynamic rotor	2
6	Interaction test, varying angle in two planes of static rotor	2
7	Interaction test, varying angle in two planes of dynamic rotor	2
8	Perpendicular interaction test	2

Chapter 4

Methods

4.1 Generalized solution

A generalized solution was suggested to comply with the functional requirements in Chapter 3, based on the literature study and conversations with senior engineers at SINTEF Ocean and NTNU.

The setup needed to include a rigid base which would represent the foundation of the floating wind turbine. This base needed to be connected to a fixed, stiff beam representing the tower of the FWT. The solution needed the ability to induce loads in all six degrees of freedom. Therefore, it was designed as a sphere with holes to attach fan arms in different configurations to be placed on top of the beam. Up to 8 fan arms could be connected at a time, and the loads would be measured by an accelerometer and a 6-component load cell fixed on top of the beam and in the center of the hub. Furthermore, the mechanical solution needed the ability to perform the functional tests mentioned in Section 3.2.

In addition, the base plate needed to be able to be attached to SINTEF Ocean's hexapod for tests with dynamic motions. The complete setup then consisted of a base, a fixed, stiff beam, an accelerometer, a 6-component load cell, the spherical hub, and the fan arms.

4.2 Preliminary technical solution

A preliminary technical setup was designed from the general solution, with additional specifics and details.

4.2.1 The base and beam

The base was intended to be a heavy steel plate that could be fixed to the surface. It needed to be rigid to avoid adding noise to the measurements. Moreover, it needed to be able to be fixed to the hexapod for tests with dynamic motions.

The beam was then intended to be welded to the base and made of steel to be as stiff as possible. An attachment for the sensors would then also be welded at the top of the beam. The beam had to be at least 0.9 m to comply with the requirement for minimum clearance to the surface with fan arms attached, as mentioned in Table 3.1.

4.2.2 Data acquisition and measurements

The 6-component load cell used for the solution needed an accuracy of at least 0.2 N for the measurements. In addition, a three-axis accelerometer was also attached to obtain more reliable velocity estimates for tests with a moving platform. Given the requirements for the max force on the structure, the accelerometer needed to handle a max acceleration of 3 g.

4.2.3 The spherical hub and connection sleeve

The spherical hub was intended to be made to accommodate the different configurations needed to test wind loads in all six DOF. The hub would be created with a hole in the bottom to connect the stiff beam with the 6-component Force-Torque Sensor. An inner plate would then be fixed to the beam so the load cell could be placed in the center. This inner plate could be accessed due to another hole in the top of the hub. The hub would be 3D-printed and designed with holes in an interval of a hole for every 15° in x-, y-, and z-direction. A connection sleeve would be fixed to the holes in the hub to attach the fan arms.

4.2.4 The fan arm

The fan arms consisted of an actuator, a propeller, and a carbon fiber arm. The fans needed the ability to connect and disconnect from the spherical hub to be configured at different angles and positions. The arms were wanted to be as light as possible while still being stiff, and a carbon fiber tube was therefore chosen as the main design. The actuator needed to be at least 0.5 m from the center of the hub, and the arms would then be, at a minimum, created at this length. The actuator and propeller combined would need to produce the necessary forces as detailed in Table 3.1.

4.2.5 The software

Arduino was planned to be used as the software to control the actuators in this setup. It needed to be compatible with the actuators and had been used as the software for multiple studies such as [23] and [26]. The software catman Easy would be used to record and visualize the resulting measurements. In addition, HexaSym would be used as the software to control the hexapod motions [31].

4.2.6 Other components

Some other components would also be needed to make the technical solution function. Firstly, to run the actuators, power supplies would be required. Each actuator would use one power supply, and eight would be needed. In addition, a signal amplifier would be needed for amplifying the signal and acquiring the data. Wires connecting the different components would also be needed, and an Arduino Mega would be needed to control the actuators.

4.2.7 Summary

Based on the literature study, the setup had to fulfill the functional requirements given in Chapter 3. To achieve this, the technical solution would be made of a rigid base, a stiff, fixed beam, an accelerometer, a 6-component load cell, a hub with attachment points, and configurable fan arms. In addition, the components mentioned in Section 4.2.6 would also be needed. A preliminary concept sketch of the technical solution can be seen in Figure 4.1. The figure was shown in 2D and was simplified in terms of actual dimensions and the number of configurations.

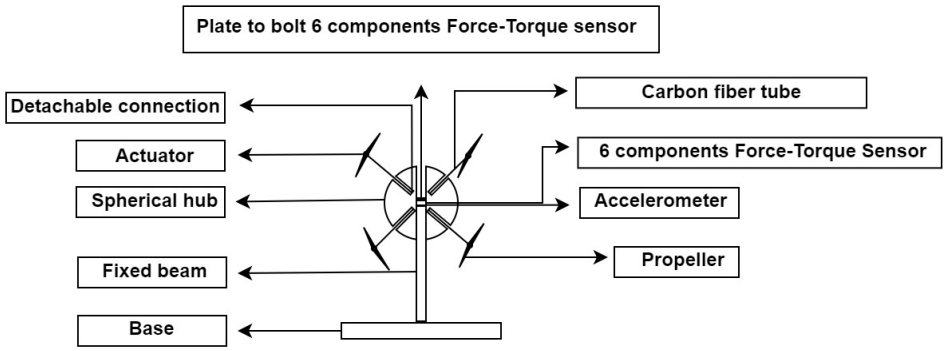

FIGURE 4.1: A concept sketch of the mechanical solution in 2D

4.3 Iteration of technical solution

The design was iterated, and additional details were added while creating the solution. This section aimed to give an understanding of this process and how the design changed.

4.3.1 The base and beam

The base of the setup was chosen to be a 1000x1000x8 mm^3 steel plate. This was a sufficient thickness for wielding the beam to the plate without using unnecessary materials. Furthermore, 80 kg of weight was added to the base to make it stiffer and give it properties closer to a fixed structure. The beam chosen was a 1.15m cylindrical steel beam with a diameter of 10 cm, where the load cell was connected at the top. The height was chosen to have the hub at a height where it would be easy

to adjust the fan configurations while having sufficient clearance from the surface. The beam's diameter was set to be shorter than the hole in the bottom of the spherical hub to ensure all forces applied to the hub would go through the load cell to avoid errors in the measurements.

The base and beam can be seen in Figure 4.2.

FIGURE 4.2: The base and beam

4.3.2 The spherical hub and connection sleeve

Trond Innset made a 3D sketch of the original design for the spherical hub, which can be seen in Figure 4.3. A 3D-printed connection sleeve was then intended to be fixed to the holes in the hub to attach the fan arms.

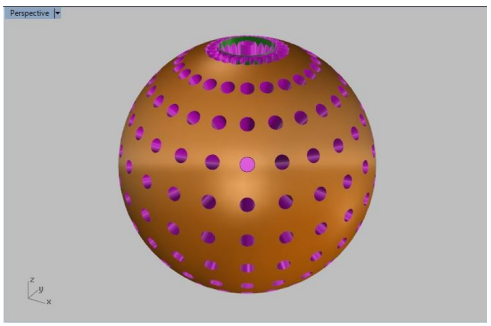

(A) The spherical hub, by Trond Innset [32]

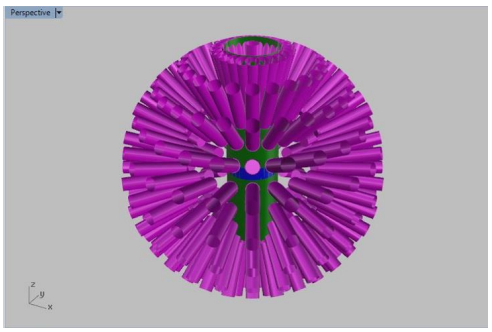

(B) The spherical hub without the outer shell, by Trond Innset [33]

FIGURE 4.3: The spherical hub

This design was then redeveloped, where the connection mechanism was included in the hub design as a protruding piece out of the hub, as seen in Figure 4.4.

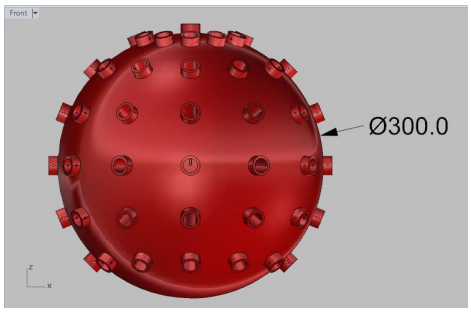

FIGURE 4.4: The spherical hub with included connection mechanism - by Trond Innset [34]

The design was then revised to make space for the load cell to be connected in the center of the hub while adding a hole in one side of the hub for the necessary wiring for the sensors. In addition, the connection mechanism was further developed. The solution was to include a thin protruding piece in the center of the holes at a fixed angle in the vertical direction. This was to verify the angle of the fan arms when configuring them to the hub. Moreover, a hole was added through the protruding part of the hub to fix the fan arms in place with a locking pin. The configurable holes were placed in an interval of a hole every 30° horizontally, and a hole every 22.5° vertically.

These details and the final version of the spherical hub can be seen in Figure 4.5.

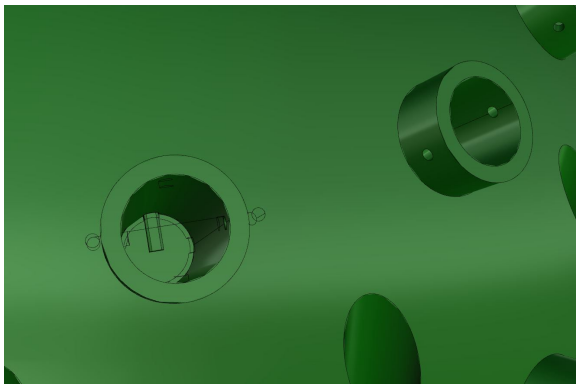

(A) The connection mechanism - by Trond Innset [35]

(B) The spherical hub, final version

FIGURE 4.5: The finished connection mechanism and the spherical hub

4.3.3 The fan arm

The fan arm design was further developed by cutting one end of the carbon fiber tube in a cross pattern at 90° to match the protruding piece in the holes. With this design, the angle of the fan arm could be chosen based on the insertion into the hub. In addition, a hole was made in the tube, matching the one made to the protruding part of the hub. This was done to fix the arm to the hub using a locking pin. It was

also needed to be able to fix the actuator to the fan arm. This was done by creating a mechanical configuration screwed together to the actuator using the screw holes in the actuator design. Furthermore, the mechanical configuration was connected to the fan arm by a grub screw. Trond Innset made the main design for the fan arm, and Ole Erik Vinje constructed the mechanical parts. The finished design can be seen in Figure 4.6.

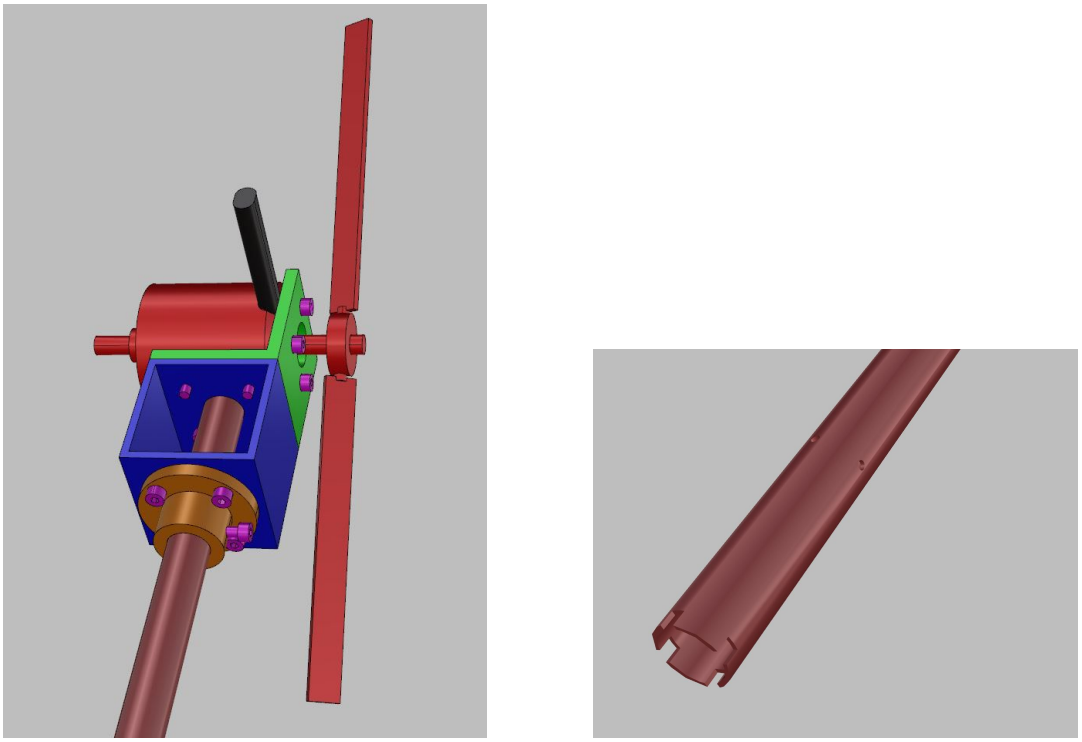

(A) The mechanical fan arm design - by Trond Innset [36]

(B) The connection design - by Trond Innset [37]

FIGURE 4.6: The fan arm design

The actuator chosen for the model was the "Odrive DUAL SHAFT MOTOR - D5065 270KV", which could produce a force of 208.49 N [38], well above the requirements needed for the tests, as mentioned in Table 3.1. The product "Karbonrør vevd 3K - 16x14x1000mm - Bronto" was chosen as the fan arm because it was a carbon fiber tube accessible in Norway at a reasonable price range. In addition, this product would be of sufficient length, as the fan arm initially was chosen to be 700 mm. The actuator needed to be at least 500 mm from the center of the hub, and by choosing a longer fan arm, it would be possible to test if the fan arms' length would affect the results.

The chosen actuator had a revolutions per minute (rpm) limit of 8000. A propeller that could produce the necessary forces for an rpm within the actuator's limit was then needed. In addition, another limiting factor for the choice of the propeller was the maximum power output of the power supplies. For this project, a maximum

power output of 960 W was chosen, as this is what SINTEF Ocean had used previously. It was also wanted to have as small of a propeller as possible to be able to set up the fan arms in as many configurations as possible without the fans touching each other. When iterating over these properties, the product "16×5.5MR" from APC Propellers [39] was chosen. The thrust force properties used for this iteration were collected from [40]. The propeller, the carbon fiber tube, and the actuator for the fan arm can be seen in Figure 4.7.

(A) 16×5.5MR, from [39]

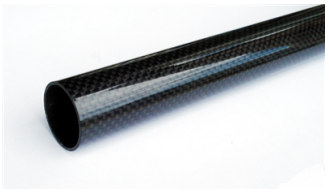

(B) Karbonrør vevd 3K - 16x14x1000mm - Bronto, from [41]

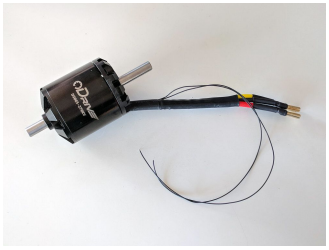

(C) Odrive DUAL SHAFT MOTOR - D5065 270KV, from [42]

FIGURE 4.7: The fan arm components

4.3.4 The software

At first, it was intended to use the software Arduino IDE to control the actuators, but this was later changed to use the built-in graphical user interface (GUI) from Odrive. The GUI was a more time-efficient solution as it removed the need for programming for static tests. Moreover, it was also possible to use Python to control the actuators if the GUI would be insufficient.

4.3.5 Other components

The Mean Well TDR-960-48 was chosen as the power supply due to its voltage and power rating matching the power supplies used for SINTEF Ocean's experiments while being at a reasonable price range. In addition, an Arduino Mega was initially chosen as the controller for the actuators, but this was changed to Odrive Pros instead. This change was due to the compatibility of using an Odrive controller with an Odrive actuator which also made it possible to use the built-in GUI from Odrive. In the Odrive GUI, the controllers were identified as Odrive 0, Odrive 1, and Odrive 2. As the controllers were connected to the same actuator throughout all tests, this naming convention will be used to differentiate the different fan arms where applicable. The wiring type was chosen to be copper cables and was used for wiring each fan arm to the power supply and an Odrive Pro. The power supply and controller can be seen in Figure 4.8.

(A) The Mean Well TDR-960-48 (B) The Odrive Pro

FIGURE 4.8: The power supply and the controller

It was later realized that the power supply worked on 3-phase power, which meant a 3-phase cable also was needed. The product Skjøtekabel h07rn-f 5x2.5 16amp 400v 416-6 25m was then chosen for this, cut to access the individual wires, and connected to the power supply. The 3-phase cable can be seen in Figure 4.9.

FIGURE 4.9: The 3-phase cable, from [43]

4.4 Instrumentation

4.4.1 The 6-component load cell

The HBM Multiaxis Force Sensor MCS10 was initially chosen and kept as the 6-component load cell due to containing the necessary accuracy of 0.2 N. In addition,

it was a component NTNU had available for use in the experiments. The load cell can be seen in Figure 4.10.

FIGURE 4.10: Multiaxis Force Sensor MCS10 - from [44]

4.4.2 The accelerometer

The 5G 3-axis accelerometer AD22293Z from Analog Devices Inc was chosen for the setup as it was a component NTNU had available for the experimental solution and contained the necessary accuracy of at least 3g. This accelerometer can be seen in Figure 4.11.

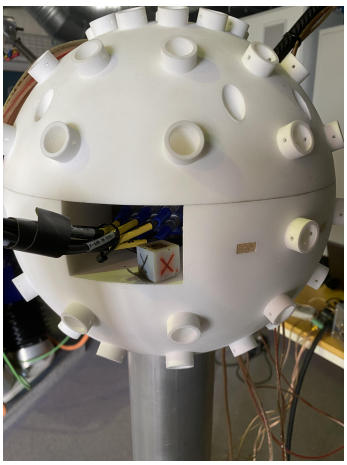

FIGURE 4.11: The accelerometer

4.4.3 The signal amplifier

The strain gauge amplifier for the setup was a bundle of an HBM QuantumX MX840B, a QuantumX MX840A, and a QuantumX CX27B, as this, in total, had enough sensor outputs for the 6-component load cell and the 3-axis accelerometer. D-SUB cables with lemo connectors connected the amplifier to the load cell and the accelerometer. An ethernet cable was also used to connect the QuantumX CX27B to the computer.

The setup for the strain gauge amplifier can be seen in Figure 4.12.

FIGURE 4.12: The signal amplifier

4.4.4 Software

The software HBM catman Easy was used to read the load cell and accelerometer data. It was necessary to reset the measurements to zero after the setup configurations were changed before running a test. This was done directly in the software. The software would then signal that the measurements were reset, and by pressing "Play", the software started to record data. The test was finished by pressing "Stop", and the software would then give the option to save the data as a .bin-file. This .bin-file could then be inputted into the software Plotme by SINTEF for analysis. Plotme was used to get plots for the different loads in the time domain and to calculate the standard deviation. Furthermore, it could also calculate a low-pass filtered version of the measurements and present the data in the frequency domain.

4.5 Final solution

The complete final solution for the experiments can be seen in Figure 4.13. The steel beam seen next to the solution in Figure 4.13a was used to making sure the wiring to the load cell and accelerometer did not touch the spherical hub, which could have affected the results. A complete components list and list of purchased components can be seen in Appendix A.

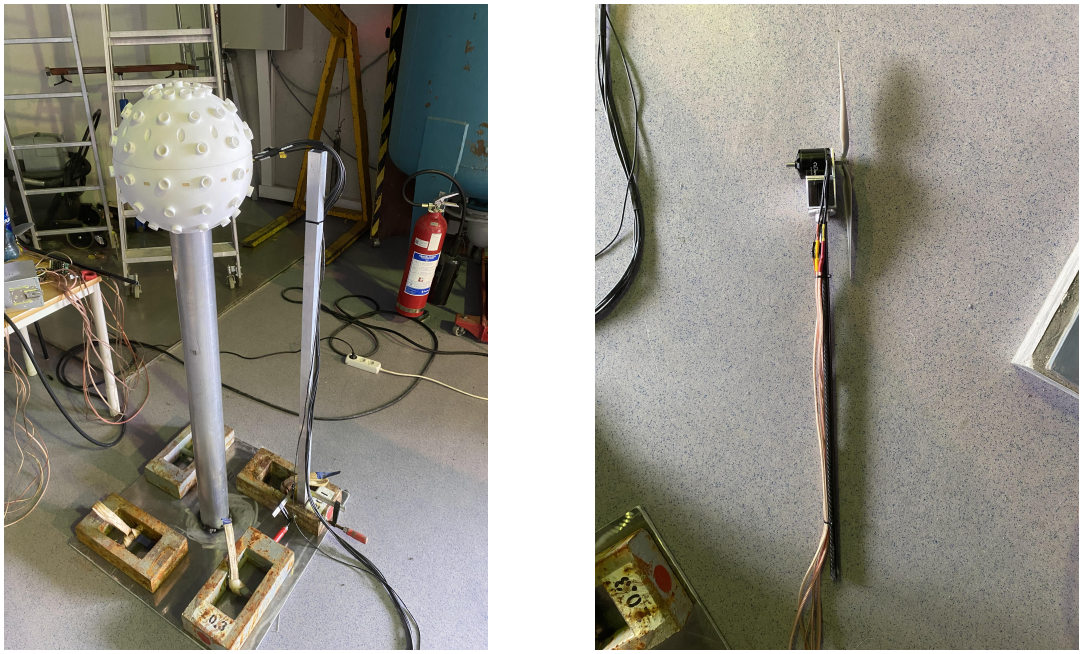

(A) Complete setup (B) The fan arm

FIGURE 4.13: The setup and fan arm

Chapter 5

Results

5.1 Functional tests

The functional tests required for the system were divided into documentation tests for validation and a test matrix for performance, as mentioned in Chapter 3. A complete test list of all performed tests can be seen in Appendix B. Each test was performed for at least 180 seconds to reduce the effect of disturbances on the measurements.

The results were presented one test at a time, with a corresponding graph where applicable and with describing notes.

5.1.1 Documentation tests

The results from the documentation tests were divided as seen in the list in Section 3.2.1.

5.1.1.1 The setup and instrumentation

The 6-component load cell was tested using a hand-held force controller to see if the measured forces and moments were calibrated correctly. This was measured by aiming the hand-held force controller in solely x-, y-, and z-direction, respectively, and reading the values for the resulting measurements. Tests were also performed for the moment, where the moment was calculated using the formula $M = F \cdot d$, where d is the distance from the axis of rotation, and the distance from the center of the setup to the induced force was measured to be 80 cm. The results were deemed equal and within the required accuracy of 0.2 N.

5.1.1.2 Software velocity test

The software used for the tests, Odrive GUI, had a status LOCKIN_SPIN, for which the actuator would spin continuously at a velocity chosen with the parameter vel. The acceleration of the system was also configurable with the parameter accel. A configuration test was performed to translate the vel parameter to rps. This test was

performed by spinning the fan at low speed and manually counting the rotations for one minute. Then the vel parameter was tweaked to get closer to one revolution per second, and the test was repeated. After a few iterations, it was found that a value of 6.9 vel equaled one revolution per second, with a deviation of less than $\frac{1}{60}$=1.66%.

5.1.1.3 Repeatability test

The same test was run at the start of each testing day with a fan arm configured as seen in Figure 5.1a, to test the repeatability of the setup. This test was performed five times for an rps of 36.23, and the resulting forces and moments with standard deviation can be seen in Figure 5.1b. Raw data for the repeatability test can be seen in Appendix C.1.

(A) The repeatability test configuration

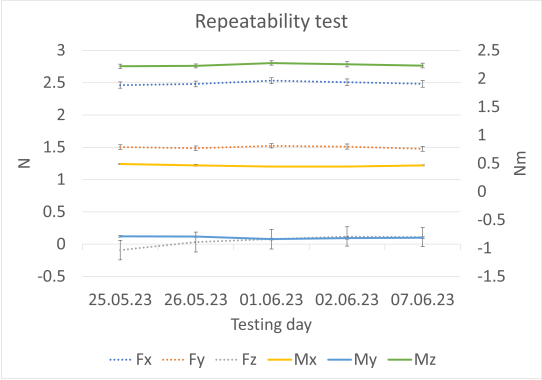

(B) Repeatability test

FIGURE 5.1: The repeatability test

5.1.1.4 Fan arm performance test

Tests were run to study whether there were individual differences between the fan arms. This was done by performing tests for the same configuration and rps with each fan arm. The fan arms were set up in configurations where forces only would be applied to the load cell in either x, y, or z-direction. Figure 5.2 illustrated these configurations.

The tests were run for increments of 30 from 0 to 450 vel in the GUI, which translated to rps was increments of 4.35 from 0 to 65.25 rps. Each measurement was run for at least 180 s, and the resulting thrust curves for the three fan arms for F_x and F_z with included standard deviation can be seen in Figure 5.3. F_y was not shown as it was

identical to the thrust curve for F_x. These thrust curves were created using Excel, and the curve-fitted polynomial was added to the plot with its resulting equation. The thrust curves for F_x and F_z can be seen to be closely related, but were not identical.

(A) The setup for thrust curves in F_x and F_z

(B) The setup for thrust curves in F_y

FIGURE 5.2: The setup for thrust curves

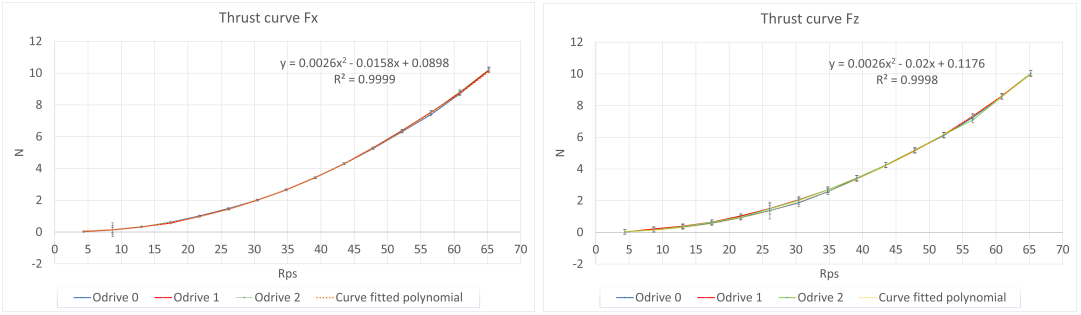

(A) Thrust curves for all fans in F_x

(B) Thrust curves for all fans in F_z

FIGURE 5.3: Thrust curves

When running the experiments, non-negligible forces were also measured in the other force directions than the one tested. This was the case for all three configurations, and no differences were observed in these measured forces between the fan arms. However, the measured forces in these directions were larger when testing with only induced load in F_z than in F_x or F_y. Measured loads for Odrive 0 with only expected load induced in F_x can be seen in Figure 5.4 to illustrate this. It can be seen that the loads increased with increased rps.

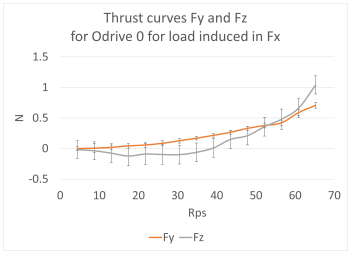

(A) The forces measured in F_y and F_z for Odrive 0 for load induced in F_x

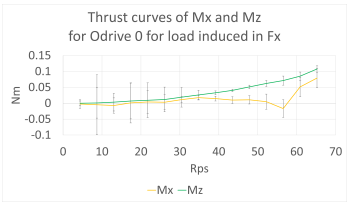

(B) The moments in M_x and M_z measured for Odrive 0 for load induced in F_x

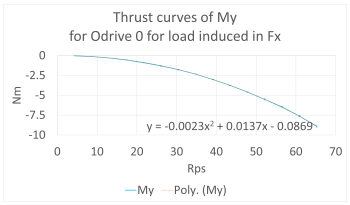

(C) The moment in M_y measured for Odrive 0 for load induced in F_x

FIGURE 5.4: Loads for Odrive 0, with load induced in F_x

In addition, tests were run to see if the fan arms performed similarly for different configurations at a fixed rps of 58. This was tested by having the fan arms induce a moment about only one direction of force and comparing the measurements for different configurations. The tested configurations of the setup were at the vertical position, at 45°, 67.5°, and 90°. 22.5° was not tested because fixing the fan arms in this configuration for the current solution was impossible. This was elaborated upon in Section 6.2. The test was performed multiple times with different fan arms, and the average moment with standard deviation can be seen in Figure 5.5. It was seen that the measured absolute value of the moment was reduced for each subsequent change in the configuration from the vertical position to a horizontal position.

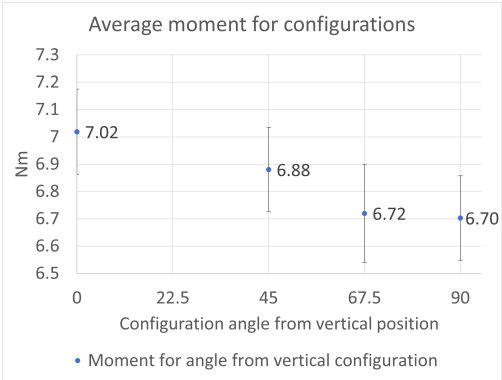

FIGURE 5.5: The average moment measured for different configurations

5.1.1.5 Hammer test

A hammer test was performed to find the eigenfrequencies of the construction by using a rubber hammer and hitting the construction at different spots to see how it would react. The software Plotme was then used to present the data in the frequency domain, as seen in Figure 5.6. It was found that the natural frequency of the setup was approximately 8 Hz, while the eigenfrequency of the fan arms was approximately 2.3 Hz.

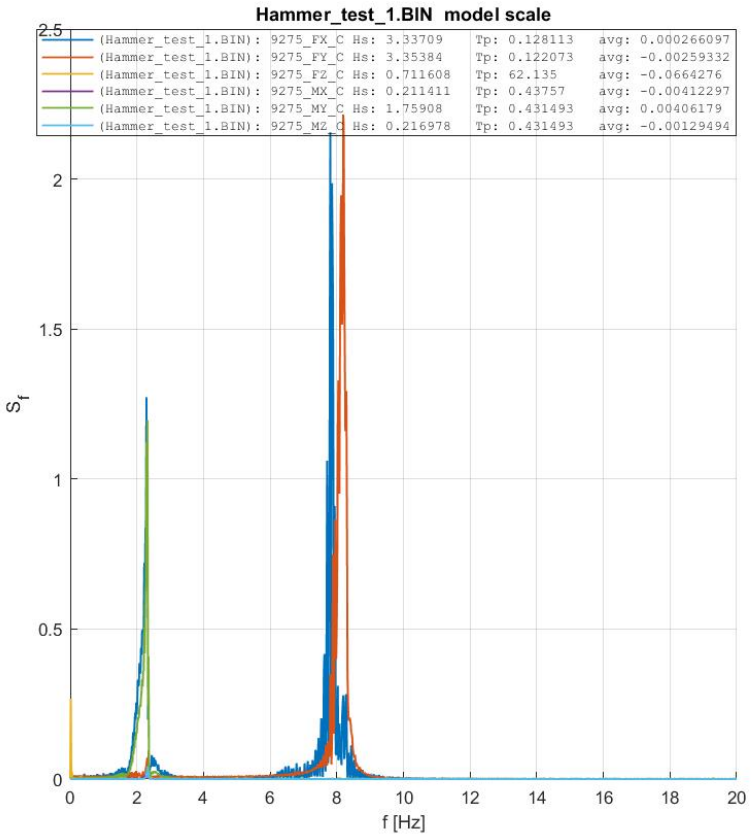

FIGURE 5.6: The hammer test, from Plotme

5.1.2 Test matrix

The results from the test matrix were split as seen in Table 3.2.

5.1.2.1 Static load test with multiple fan arms in parallel configuration

Tests were run to see the effect simultaneously running multiple actuators would have on the resulting forces and moments. Firstly, a test was executed with two fans set up in parallel at 45° to each side as seen in Figure 5.7. The test was run by running both actuators simultaneously for a rps of 58, and comparing the results to the measurements for each actuator run separately, added together. The resulting loads can be seen in Figure 5.8.

FIGURE 5.7: Static load test in parallel configuration

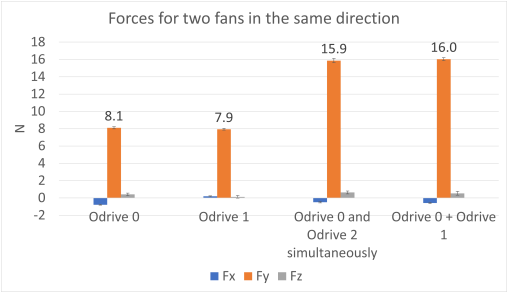

(A) Measured forces for the static load test in parallel configuration

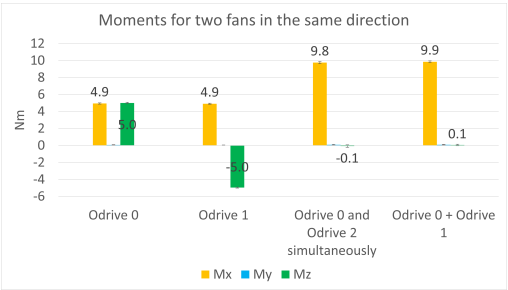

(B) Measured moments for the static load test in parallel configuration

FIGURE 5.8: Measured loads for the static load test in parallel configuration

5.1.2.2 Static load test with multiple fan arms in opposite configuration

Tests were run to see the effect simultaneously running multiple actuators in opposite directions would have on the resulting forces and moments. The test was executed with two fans set up at 45° to each side, directed opposite from each other, as seen in Figure 5.9. The test was run by running both actuators simultaneously for a rps of 58, and comparing the results to the measurements for each actuator run separately, added together. The resulting loads can be seen in Figure 5.10.

FIGURE 5.9: Static load test in opposite configuration

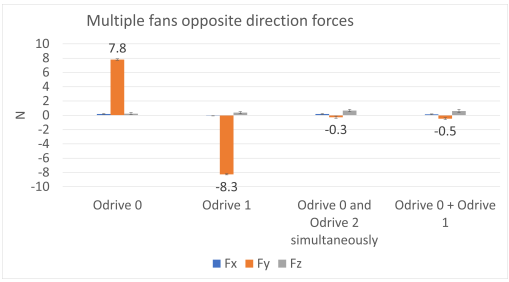

(A) Measured forces for the static load test in opposite configuration

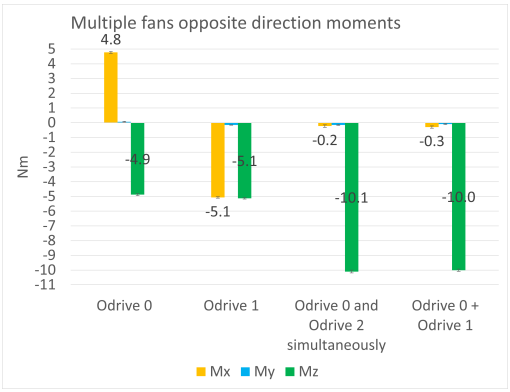

(B) Measured moments for the static load test in opposite configuration

FIGURE 5.10: Measured loads for the static load test in opposite configuration

5.1.2.3 Interaction test, varying angle of static rotor

An interaction test was performed with one actuator running to measure the effect of configuring the fan arms near each other. The test was performed for multiple configurations, with a static fan arm configured in front or behind the running actuator. The rotor was held constant at 58 rps for this test. The static fan arm was configured behind and in front of the running rotor, for angles of 22.5°, 45°, and 67.5° away from the running rotor. Plots showing the interaction effect can be seen in Figure 5.11.

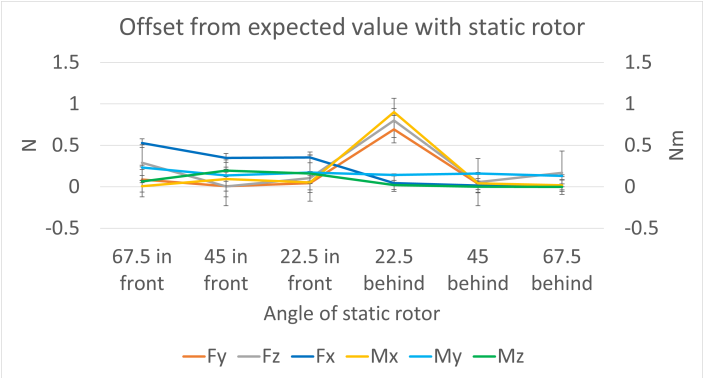

FIGURE 5.11: Measured performance difference of loads for the interaction test with varying angles of the static rotor

These results showed a noticeable interaction for the angle configuration of 22.5° for the static rotor when placed behind the running actuator. Furthermore, there seemed to be negligible interaction when placing the static fan arm 45° or more behind. There seemed to be an offset for forces in F_x when the rotor was placed in front, but the other loads were unaffected.

5.1.2.4 Interaction test, varying rps

A test was also performed to see the effect changing the rps of the setup would have. The test was run with a static rotor configured 22.5° behind the running actuator, configured horizontally. The test was run for rps of 4.35 to 65.25, with increments of 4.35, and was compared to the thrust curve to calculate the offset. The results can be seen in Figure 5.12, showing that the expected value's offset increased with increasing rps.

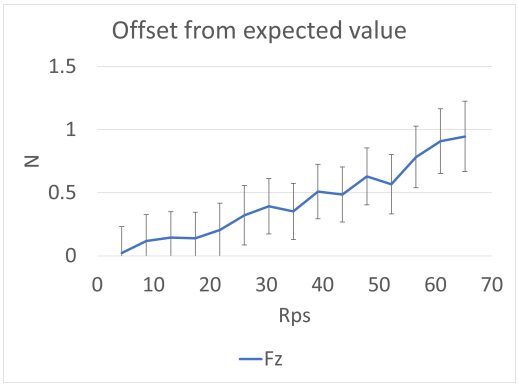

FIGURE 5.12: Measured performance difference of loads for the interaction test with varying rps

5.1.2.5 Interaction test, varying angle of dynamic rotor

An interaction test with two actuators running, configured in angles of 22.5°, 45°, and 67.5° behind each other, was also performed to inspect the interaction effect.

Both actuators were held constant at 58 rps for this test. Plots that show the offset from the expected values can be seen in Figure 5.13.

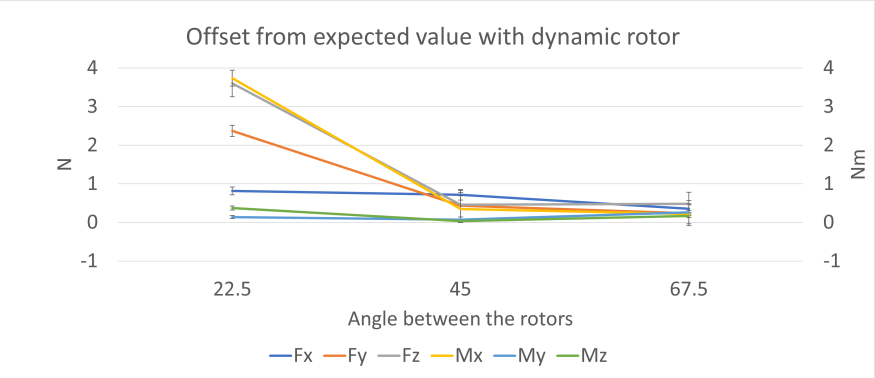

FIGURE 5.13: Measured performance difference of loads for the interaction test with varying angles between the rotors

These results showed a noticeable interaction for the loads for angles of 22.5° between the two rotors. In addition, there might have been a slight interaction effect for 45°. It was also noted that the standard deviation was large at this angle. For 67.5° angle between the rotors, however, there did not seem to be an offset from the expected value.

5.1.2.6 Interaction test, varying angle of static rotor in two planes

An interaction test where the rotor was configured in two planes was also performed. The rotor was configured behind and to the side of the running actuator, as illustrated in Figure 5.14. The actuator was held constant at 58 rps for this test. The starting placement was chosen based on the results in Section 5.1.2.3, which stated that there was an interaction when the static rotor was placed 22.5° behind the running actuator. This was then used to determine how far to the side the fan arm had to be moved for there not to be an interaction anymore. The resulting plots can be seen in Figure 5.15.

FIGURE 5.14: Configuration of the static rotor 22.5° behind and 30° to the side of the dynamic rotor

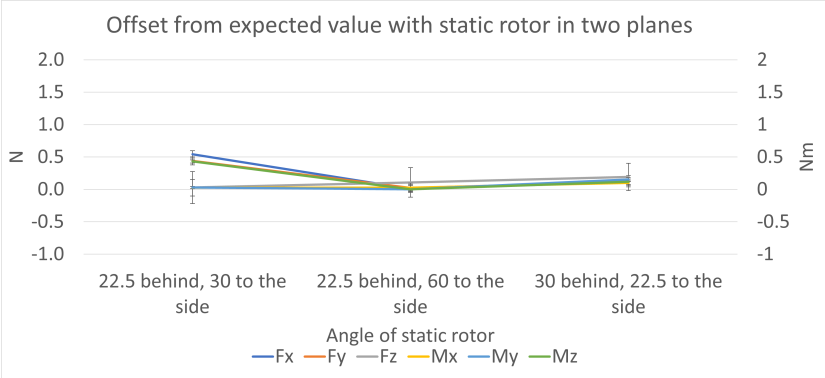

FIGURE 5.15: Measured performance difference of loads for the interaction test with varying angles of the static rotor in two planes

These results showed that when the fan arms were moved 30° to the side for the configuration of 22.5° behind, there might still be a slight interaction effect, but for 60° to the side and 22.5° behind or 22.5° to the side and 30° behind, there did not seem to be a jet interaction.

5.1.2.7 Interaction test, varying angle of dynamic rotor in two planes

The previous test was also performed with a dynamic rotor, with both rotors held constant at 58 rps for this test. The resulting plots can be seen in Figure 5.16.

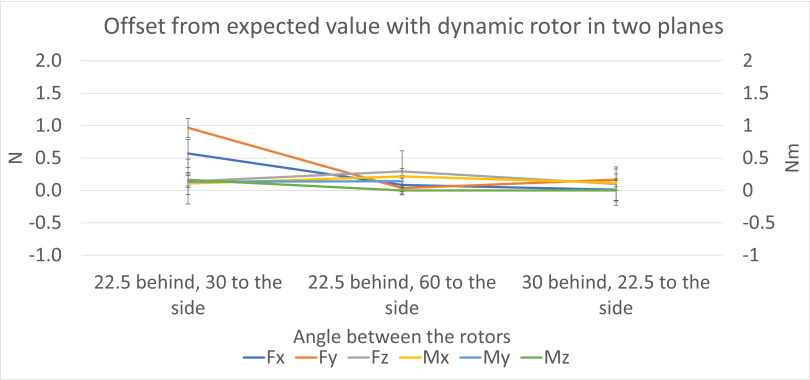

FIGURE 5.16: Measured performance difference of loads for the interaction test with varying angles of the dynamic rotor in two planes

These results showed an offset in the loads when the fan arms were moved 30° to the side and 22.5° behind, but no large offset for 60° to the side and 22.5° behind or 22.5° to the side and 30° behind. In addition, an increase in the standard deviation was noticed for all configurations compared to tests with a static rotor.

5.1.2.8 Perpendicular interaction test

A perpendicular interaction test was also performed, with both fan arms running perpendicular to each other. The actuators were held constant at 58 rps for this test, and 45°, 67.5°, and 90° angles between the rotors were tested. In addition, tests where one fan arm was configured 45° away and 30° to the side and 67.5° away and 30° to the side compared to the other fan arm were also tested. Figure 5.17 illustrated the setup for 90° angles between the rotors. The resulting plots for this test can be seen in Figure 5.18.

FIGURE 5.17: Configuration of perpendicular interaction test with 90° angle between the rotors

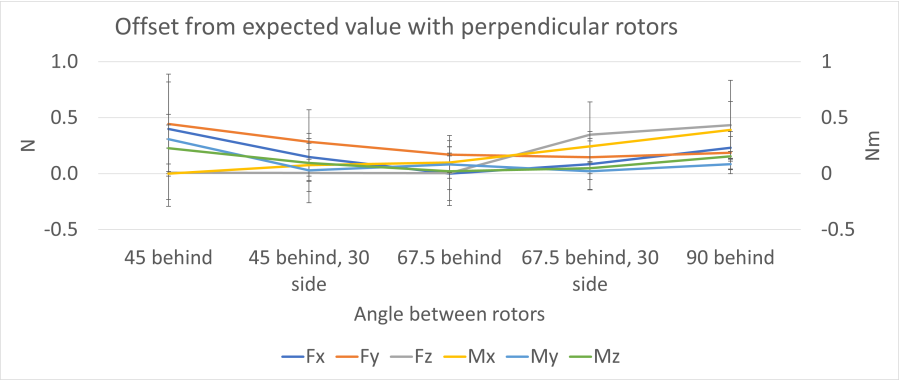

FIGURE 5.18: The perpendicular interaction test loads

There was no large interaction effect for the perpendicular interaction test. However, there might have been a slight offset for the configuration of 45° angle, and the standard deviation was significantly increased. When the angle between the fan arms was increased, or one of the fan arms was moved to the side, the standard deviation was noticed to be reduced, but was still higher than for other tests with two dynamic rotors.

Chapter 6

Discussion

6.1 Functional tests

6.1.1 Documentation tests

6.1.1.1 The setup and instrumentation

The setup was tested with a hand-held force controller as mentioned in Section 5.1.1.1. This test was run under the supervision of Robert Opland to verify if the recorded measurements of the load cell were reliable, and if it had been calibrated correctly. There will always be some uncertainties when using a hand-held instrument, as a human would perform the test and read the values. However, the hand-held and calculated measurements were sufficiently similar, and the accuracy was verified to be within the required value of 0.2 N. As the setup was deemed to measure the loads correctly, the reliability of measurements for the other tests was increased.

6.1.1.2 Software velocity test

As mentioned in Section 5.1.1.2, the software used the parameter vel to control the rotational speed of the actuator, which corresponded to the fan speed. This test was performed to translate the vel parameter to revolutions per second for a more intuitive understanding of the fan speed. It was seen that the rotational speed of the actuator was increasing linearly with vel, and a direct translation between the two variables was then possible to calculate. As mentioned, this test showed that 6.9 vel was equal to 1 rps.

As the test was performed by counting revolutions manually over an extended period, the result included human error and accuracy uncertainties. However, the result was deemed reliable with an error of less than 1.66%, as the test was run multiple times for 1 minute and gave the same results. These results were then used to translate the software parameter vel to rps for the other tests.

6.1.1.3 Repeatability test

A test was repeated each testing day to measure the repeatability of the solution. This configuration was chosen because it induced forces and moments in multiple directions and not just in one. For the setup, it also made sense to measure larger forces in F_x than F_y as the configuration angled the fan more in the x-direction than in the y-direction. Furthermore, both F_x and F_y would mostly contribute to a moment in M_z, with a smaller contribution in M_x as well. The fact that F_z and M_y were negligible also corresponds with the theory for this configuration, and the test seemed to induce the correct loads. As mentioned, it was seen that the values for the loads were the same for each repetition. This then increased the setup's reliability, as it could be expected that other tests also would behave similarly for repetitions.

6.1.1.4 Fan arm performance test

The fan arm performance test was run to verify if there were any differences in performance between the fan arms and in different load directions. In addition, the thrust curves were created from the measurements and would be used as a benchmark to measure the performance of the fans for other tests.

From the thrust curves seen in Figure 5.3, it was seen that the fan arms were performing very similarly for both F_x and F_z. However, it was also noticed that there are some differences between the two thrust curves. The measured load induced in F_z was less for all fans than F_x. This was explained by the stiffness of the fan arms. When the fan arms were exposed to a perpendicular force, they started to bend slightly, which then caused the force induced by the fans to change direction. Because of this, the load cell measured forces in multiple directions, not only in the intended one. Since the fan arm was set up horizontally for the test of F_z, as seen in Figure 5.2a, the weight of the fan arm caused it to start to bend before thrust was applied. This caused the total bending of the fan arm when measuring force in F_z to be larger, which caused the measured force to be slightly lower than for the tests of F_x and F_y configured in the vertical position. At the same time, greater forces were also measured in the other directions, as the increased bending would change the angle of the fan arm more toward those directions.

The results in F_x and F_z would have been more similar if the fan arms' stiffness were increased or their weight was decreased. Furthermore, there were also larger individual differences between the fan arms for the results in F_z. This can be seen in the thrust curves in Figure 5.3, where there was less overlap for the tests in F_z. This difference was due to the different wiring used for the fan arms, which had different weights. This caused the initial bending to be different for the horizontally configured fan arms before the start of the test. In addition, the standard deviation was also greater for F_z. This was due to the higher precision of the load cell in F_x and F_y than for F_z. Moreover, the fan arms performed identically for the tests in F_x and

F_y. This was to be expected, as the precision was equal for F_x and F_y, and the vertical configuration was chosen for the thrust curves for both tests.

It can also be seen that the measured loads in the unintended directions mostly increased with increasing rps. There seemed to be some uncertainty for lower rps, particularly for F_z. However, for rps of 50 and higher, there seemed to be a non-negligible effect that rapidly increased with the rps. This indicated that the bending of the fan arms increased non-linearly with higher induced loads.

From the fan arm performance tests, it was concluded that the difference between the fan arms was minor and that they were interchangeable for the different tests.

It was also noted that the fan arms induced different moments for different configurations, which were reduced for each increment lowered from the vertical position. This was because, before each test, the measured loads on the setup were reset to 0. This included the load from the weight of the fan arms. Then, when the fan arm induced a load, it would bend slightly, which shifted the center of mass of the fan arms. This change in the center of mass would add to the moment measured by the load cell and be an error source for the measurements.

The error would be the largest for the vertical configuration. The bending when the fan arm induced a force at this configuration would change the moment arm of the fan arm from zero to non-zero. This change would cause a larger effect than, for instance, the horizontal position, where the change in position due to bending only would cause a slight relative change in the moment arm, as the original moment caused by the weight of the fan arm was already taken into account when the measurements were reset. This explained why the moment was the largest at the vertical position and why the values decreased with changes in configurations away from the vertical position.

6.1.1.5 Hammer test

A hammer test was used to find the natural frequencies of the setup by using a rubber hammer and hitting the construction at different spots to measure the vibrations. As mentioned in Section 5.1.1.5, by using the software Plotme, it was found that the eigenfrequency of the construction was approximately 8 Hz, and the eigenfrequency of the fan arms was approximately 2.3 Hz. The natural frequencies were not an issue for the static tests, but would have to be kept in mind for future dynamic tests. Changes to the eigenfrequencies might have to be made if dynamic tests were to be in these frequency ranges. A solution could then be to increase the stiffness of the setup and the fan arms.

6.1.2 Test matrix

6.1.2.1 Static load test with multiple fan arms in parallel configuration

A test was performed to look at the effect using multiple actuators simultaneously would have on the results. By testing two actuators in a parallel configuration, it was expected that the force in F_y and the moment in M_x would be twice as large as each of the two when tested individually, and that the resulting moment in M_z would be 0 due to the two actuators canceling each other out. In addition, it was expected to not be induced forces in F_x and F_z.

As seen in Figure 5.8, this also seemed to be the case, with some noticeable forces being measured in F_x and F_z for Odrive 0. In addition, the results were not completely equal, as F_x was 8.1 N for Odrive 0 while Odrive 1 was at 7.9 N. These results could be explained by the weight of the fan arms being different because the wiring used was unequal. As explained previously, the fan arms were bending slightly due to their weight, which would change the angle of the induced forces and could be why the measurements differed. However, the difference was relatively small and could also be because of other error sources in the setup. In addition, the moments seemed to correspond quite well with the expected results. The standard deviation of the results was also small, and the setup seemed to be able to perform tests with two actuators running simultaneously in the same direction.

6.1.2.2 Static load test with multiple fan arms in opposite configuration

A static load test with two fan arms in opposite directions was also performed. It was expected that the resulting force would be equal to 0 N when running both actuators and that the resulting moment M_z would be twice as large as when running each actuator separately, while M_x and M_y would be negligible. The results seemed to mostly correspond with this, however, the resulting force for F_y for Odrive 1 was noticeably larger than for Odrive 0. This seems to be an inaccuracy of the fan arms, as the forces in F_x and F_z for Odrive 0 were not increased, which would have been expected if it was due to the increased bending of the fan arm.

The measured moments were also slightly smaller for Odrive 0 than Odrive 1, which was expected for the smaller induced thrust force. Furthermore, the measured moments seemed to correspond very well with the expected results when adding the results for each separate run and comparing them to the simultaneous test, as seen in Figure 5.10. In general, tests using two fans simultaneously did not seem to behave differently than tests with only one fan, which increased the reliability of the setup.

6.1.2.3 Interaction test, varying angle of static rotor

An interaction test was performed with one actuator running to measure the effect of configuring another fan arm close by. This was tested to determine which configurations would be possible to use without jet interaction effects. As seen in Figure 5.11, having a static rotor set up 22.5° behind the running actuator caused a strong interaction, but not for configurations of 45° or 67.5° behind.

There seemed to be some disturbance for F_x when the static fan arm was set up in front. However, this disturbance seemed to be an error source since the offset was larger when the configurations were further away from each other. Moreover, when calculating the offset, F_x was supposed to be 0 N for all three tests with a static rotor set in front, and this offset then showed the uncertainty of the solution with induced forces in unexpected directions. The disturbance for F_x was then seen as an error source and not considered a confirmation of noticeable disturbance when a static fan arm was set up in front for tests. There did not seem to be a disturbance for the other loads with a static fan arm in front. When the fans were spinning, they created an air wake behind, which seemed to be disturbed by the static object, but were unaffected by objects in front.

An additional test should have been run for this test. The static rotor should have been tested for the configuration of 30° behind to provide further insights into the interaction effect.

6.1.2.4 Interaction test, varying rps

This test examined the effect varying the rps would have on the interaction effect. The configuration with the static rotor configured 22.5° behind the spinning actuator was chosen as this was shown to cause an interaction effect for an rps of 58. This could then be used to see the effect changing the rps would have. From Figure 5.12, it was seen that the increasing rps caused an increase in the offset from the expected value. This indicated that the interaction effect was increasing with increased rps and with closer proximity to another fan arm. Only F_z was presented in the results as this was the induced direction of force for the test and would be sufficient to determine if there were an interaction effect.

6.1.2.5 Interaction test, varying angle of dynamic rotor

When running the interaction test with two dynamic rotors, it was seen that the offset at 22.5° angle between the rotors was much larger than for the static test. This meant that dynamic disturbances in front of the actuators would affect the results. Furthermore, there might be a slight interaction effect at 45° for the dynamic test, but this effect was much smaller than for 22.5°. This could have been an interaction between the fan arms or a part of the general inaccuracy of the setup. In addition,

there was a noticeable increase in the standard deviation for the tests with multiple dynamic rotors compared to one static. The heightened standard deviation was also noticeable for 67.5°. However, the offset from the expected values was minimal and was considered a part of the inherent inaccuracy of the setup.

A test with a 30° angle between the rotors should also have been tested to see if there would be an interaction effect at this distance. This would have given further insights into the performance of the solution.

6.1.2.6 Interaction test, varying angle of static rotor in two planes

A test was performed to see how the interaction effect would change by moving the static rotor both to the side and behind the spinning actuator. The interaction test with the static rotor configured 22.5° behind and 30° to the side of the running actuator seemed to reduce the interaction effect seen in Figure 5.11. However, there might still have been an effect that was not due to the general inaccuracy of the setup.

There did not seem to be a noticeable effect for the configuration of the static rotor 22.5° behind and 60° to the side or 30° behind and 22.5° to the side. This seemed to imply that changing the configuration 60° to the side would remove all static interaction effects. Moreover, it was noted that the closest configuration with a static rotor with no interaction effects was configuring it 30° behind and 22.5° to the side.

6.1.2.7 Interaction test, varying angle of dynamic rotor in two planes

By configuring the dynamic rotor 22.5° behind and 30° to the side of the running actuator, the interaction effect seen in Figure 5.13 was reduced significantly. However, there was still a noticeable interaction effect at this angle, as seen in Figure 5.16.

There did not seem to be a noticeable effect when configuring the dynamic rotor 22.5° behind and 60° to the side or 30° behind and 22.5° to the side. This implied that changing the configuration 60° to the side would remove the interaction effect, even with multiple dynamic rotors. Furthermore, it was noted that the closest configuration with no interaction effect was configuring the dynamic rotor 30° behind and 22.5° to the side.

In addition, the standard deviation was seen as higher for the dynamic rotor tests than for the static rotor tests. This was the case for all the configurations and seemed to be an effect of increasing the loads induced on the setup.

6.1.2.8 Perpendicular interaction test

There was not a large interaction effect noticed when running the perpendicular interaction test. However, the standard deviation for the measurements was heightened compared to all other results. The perpendicular fan arms also caused more disturbances than noticed for the other tests with two actuators. This seemed to indicate that when the two wakes were directed perpendicularly, this caused more significant disturbances than when directed in the same direction. Moreover, the expected value for a 45° angle between the two rotors might be slightly offset. At the same time, this offset could also be due to inaccuracies in the setup. Interaction effects seemed to depend on the configurations and were reduced when the fan arms were moved further apart for all other tests. The results in this test, on the other hand, were quite similar for all configurations. This then seemed to indicate that the offsets seen in the perpendicular interaction test were due to the inaccuracy of the setup.

6.2 Other observations

Currently, the setup would not be able to perform a complete cyber-physical experiment. Firstly, the measurement errors caused by the bending of the fan arms would cause the results to be too inaccurate. In addition, to perform a cyber-physical test, at least six fan arms would be needed to induce uncoupled forces in all six DOF.

The standard deviation was noticed to be heightened when running tests with multiple dynamic rotors, compared to tests with one static rotor. This was the case for all tests and seemed to indicate that an increased load induced on the setup increased the standard deviations of the measurements. This might be an issue for tests with more fan arms and higher induced loads.

In addition, the software crashed at times. Different error messages were returned, including "UNBALANCED_PHASES", "DC_BUS_OVER_VOLTAGE" and "DC_BUS_OVER_REGEN_CURRENT". "UNBALANCED_PHASES" was an error message due to some of the wirings having a too high resistance, which meant it had to be changed to a different type to be able to run the tests. This was what initially caused the wiring to be different for the different fan arms, as only some of the wires had to be changed.

The error message "DC_BUS_OVER_VOLTAGE" was returned if the chosen acceleration of the fan arms in the software was set too high, and the actuator would stop. This error message was also displayed when the actuator velocity exceeded the controller's capabilities. For the maximum velocity of the actuator, the fan arm produced a force of approximately 10 N, which was not enough as the requirement for the setup for force was 40 N. This error was connected to the power supply of the system. In the GUI, there was an option to choose the amount of voltage and

current each controller was allowed to draw from the power supply. If more power supplies were used, each actuator could draw out a higher current, and these values could be set higher. For the power supply used in this thesis, the acceleration of the fan arms was set to a level to avoid this error, which would be too low to follow the signal for dynamic tests accurately.

Furthermore, specific configurations of the setup were not possible to test. For the configurations of 22.5° from the vertical position, it was impossible to fix the fan arms in place due to insufficient space to insert the locking pins. Results for these configurations would then be unreliable before this was fixed.

In addition, an encoder would be needed for accurate control at high speeds. It was not needed for the static tests performed as the fan speed was set and did not need to be controlled in real-time, but would be necessary for dynamic tests where control at high speeds would be critical.

6.3 Error sources

There were multiple error sources in the solution. A significant error source was the uncertainty of the stiffness of the components. The stiffness was causing the angles of the induced forces to change, which caused loads in multiple directions. This caused a particular problem for the induced moment depending on the configured angle, as the more vertical configurations were subject to larger errors due to the bending.

Another error source was that using multiple fan arms simultaneously caused the standard deviation of the measurements to increase even without interaction between the actuators. The standard deviation seemed to increase with total induced load, which would cause the uncertainty to increase with each added fan arm used simultaneously.

Furthermore, the fan arms had different weights. This caused inaccuracies in the results as the heavier fan arms would bend more in different configurations than the lighter ones. This created a difference in induced loads between the fan arms. The difference in weight was due to the different types of wiring used to connect the actuator to the controller and power supply. This difference would also cause the inertia of the fan arms to be different, which could be an error source for testing with dynamic motions.

Another error source was human error. There was a possibility that measurements had been misread or miswritten when gathering the data in Excel. In addition, both the test using the hand-held force controller and the software velocity test were tests where human error could cause significant errors in the results.

In addition, assembling the mechanical parts of the fan arms was a possible error source for the setup. When screwing the components together, there could be some slight differences in the angles between the different fan arms. However, this error source seemed relatively small since the performance of the fan arms was similar when not affected by the difference in weight, as mentioned in Section 5.1.1.4. Moreover, the assembling of the mechanical parts could also be considered to be a human error.

The eigenfrequencies might also be an error source if the demanded loads would be in those frequency ranges. This was not the case for the static tests, but it might be an issue for dynamic testing.

Furthermore, the protruding parts where the fan arms were connected to the 3D-printed hub seemed to flex slightly when exposed to loads, and it was not just the fan arms that were bending. This would increase the error in the angles of the fan arms and decrease the setup's accuracy.

In addition, the bottom plate was slightly bent in the welded connection with the steel beam. This bending was another uncertainty that could cause the setup to be less stable than intended and could cause errors.

Chapter 7

Conclusion

This master's thesis aimed at designing, building, and testing an experimental setup using a multi-fan-based actuation method to test the feasibility of applying aerodynamic loads on an IEA 15 MW floating wind turbine with fans. A literature study was performed to understand the functional requirements of the setup and understand which tests would need to be performed. A solution was then made, consisting of a 3D-printed hub on a steel base and beam with configurable fan arms.

The functional tests performed on the setup provided insights into its performance and reliability. The documentation tests showed that the fan arms induced consistent measurements across repetitions and that there were minor performance differences between the fan arms, which would make them interchangeable for different experiments. Adjustments to fan arm stiffness or weight could mitigate the performance differences. Furthermore, it was seen that the induced moment was changing based on the configuration. This measurement error was the largest at the vertical position, due to the largest relative change of the moment arm.

The test matrix experiments gave valuable insights as well. The interaction tests highlighted the impact of configuration and rotor speed on jet interaction, with closer configurations and higher speeds causing larger interaction effects. In addition, the standard deviation was noticeably increased for tests with multiple dynamic rotors, which showed the effect increasing the loads had on the measurements. The perpendicular interaction test did not show significant deviations from the expected values, but displayed an enlarged standard deviation for all measurements.

The setup performed the static tests with a high degree of repeatability. However, the results had significant inaccuracies due to the bending of the fan arms, which caused loads to be measured in multiple directions.

The solution would not be suitable for performing dynamic tests. Firstly, more fan arms would be needed to perform experiments with dynamic loads in 6 DOF. Moreover, the acceleration and velocity limits of the setup would not be sufficient for

the dynamic tests, and a more powerful power supply would be needed. In addition, the uncertainty of the bending of fan arms when inducing loads would have to be addressed for these tests. Design changes and improvements would have to be made to use the experimental solution for cyber-physical testing on an IEA 15 MW FWT.

Chapter 8

Further work

8.1 Improvements of the setup

There were multiple ways to improve the setup. Firstly, the fan arms needed to be stiffer. The bending of fan arms would have to be taken into consideration when running the hybrid tests. A solution for cyber-physical testing could be to angle the actuators while they were running to mitigate the change in the angles. However, this solution would need to know the fan arm angle in real-time to adjust the actuator angle accordingly. The change in the measured length would also have to be considered, as when the carbon fiber tube was bending, the moment arm between the induced force and the center of the hub would change, affecting the induced moments. A way to stiffen the carbon fiber arms could be to shorten the distance, but this would increase the interaction effect when using multiple fan arms as they would be configured closer.

In addition, the general setup could also be stiffer. This was not an issue for the static tests, but could pose an issue when running dynamic tests due to the setup's natural frequency. A way to increase the stiffness could be to weld inclined steel beams to the bottom plate and the beam.

Another setup improvement would be to use thinner wiring between the fan arms and the controller, as this would reduce the weight. The thinner wiring would be helpful to reduce the initial deformation of the fan arms and reduce the inertia of the setup when running dynamic tests. In addition, another improvement would be to use the same wiring for all fan arms, which would give the different fan arms the same weight. This would then reduce the error this difference would cause.

Furthermore, the bottom plate was slightly bent in the connection with the steel beam due to the welding, as mentioned in Section 6.3. This bending was another uncertainty that could be improved for the setup.

Another improvement would be to create holes in the protruding parts of the setup configurations at 22.5° from the vertical position so it would be possible to fix the fan

arms in these configurations with locking pins. This would give increased flexibility in which configurations to use for different tests.

8.2 Further testing

Multiple other tests would have been interesting to have tested. Firstly, testing the setup with dynamic wind loads would provide further insights. It would have been insightful to see how well the fan arms could follow the signal and if testing for all 6 DOF simultaneously would be possible. Moreover, comparing the dynamic test results to SINTEF Ocean's CDPR solution would have been interesting.

It would also have provided further insights to do experiments with more fan arms simultaneously. It would have been interesting to see how this would affect the results and the standard deviation. In addition, running tests with the hexapod would have provided a better understanding of the solution's capabilities. It would have been insightful to see how the setup would handle dynamic motions, particularly combined with dynamic wind loads.

However, none of these tests would be accurate with the current setup, but observing these results after design improvements would have been interesting. Furthermore, it would have been insightful to see how the design improvements mentioned would cause changes to the results in the fan arm performance tests or the different interaction tests.

Moreover, seeing the fan arms run at higher accelerations and velocities would have been interesting. How the jet interaction would have been affected by increased velocities would provide further insights into the interaction effect.

In addition, it would have been beneficial to perform the interaction test with varying angles of the static rotor with the static rotor placed 30° behind the running actuator to provide additional understanding of the interaction effect. It would also have been insightful to have performed the interaction test with two dynamic rotors at a 30° angle between the rotors.

It could also have been interesting to see the effect of running tests with shorter fan arms. It would be assumed that the wake interaction between fan arms would increase if the configurations were kept the same, and that the stiffness would improve.

8.3 Other

To be able to run dynamic tests, it would be necessary to gather wind data and calculate the scaled forces that would be applied. Furthermore, a script would be needed to make the fan arms follow the dynamic signal in real-time. In addition, a

thrust allocation would have to be implemented to induce the correct resulting loads in all DOF. The software HexaSym would also be needed to control the hexapod for the tests with the hexapod motions.

Appendix A

Component list

A.1 Complete component list

TABLE A.1: Complete list of components

Product	Number of units
Odrive DUAL SHAFT MOTOR - D5065 270KV	3
Karbonrør vevd 3K - 16x14x1000mm - Bronto	3
16×5.5MR	3
3D printed Spherical hub	1
Locking pin	3
HBM Multiaxis Force Sensor MCS10	1
HBM QuantumX MX840A	1
HBM QuantumX MX840B	1
QuantumX CX27B	1
D-SUB cable	9
Ethernet cable	1
5G 3-axis AD22293Z	1
Mean Well TDR-960-48	1
3-Phase Power Supply Cable	1
Solid steel plate (1000x1000x8 mm^3)	1
Solid steel beam (1150x(Diameter))	1
Odrive Pro	3
USB-A to USB-C cable	3
USB Isolator	1
3-Port USB hub	1
Cobber wires	19

A.2 List of purchased components

TABLE A.2: Complete list of purchased components

Product	**Price per unit**	**Price per unit (NOK)**	**Number of units**	**Website link**	**Total Price**
Odrive D5065 270KV	89 €	1024.10 NOK	3	https://eu.odriverobotics.com	3072.30 NOK
ODRIVE PRO	229 $	2429.87 NOK	3	https://odriverobotics.com	7289.61 NOK
16384 CPR ABSOLUTE RS485 ENCODER	59 $	625.86 NOK	3	https://odriverobotics.com	1877.58 NOK
Karbonrør	275 NOK	275 NOK	3	https://www.elefun.no	825 NOK
16×5.5MR	8.31 $	87.83 NOK	12	https://www.apcprop.com	1053.96 NOK
16×5.5MRP	8.31 $	87.83 NOK	12	https://www.apcprop.com	1053.96 NOK
ADAPTER RINGS (E)	2.69 $	28.94 NOK	4	https://www.apcprop.com	115.76 NOK
3D print Spherical hub	20000 NOK	20000 NOK	1	https://www.prototal.no/	20000 NOK
TDR-960-48 - DIN Rail Power Supply	2942 NOK (exc. VAT)	2942 NOK	3	https://www.elfadistrelec.no	8826 NOK
Skjøtekabel	8.31 $	1729 NOK	1	https://www.megaflis.no	1729 NOK
USB-hub 3 x USB-A	199.90 NOK	199.90 NOK	1	https://www.clasohlson.com	199.90 NOK
Summary	-	-	46	-	46043.07 NOK

Appendix B

Test list

B.1 Complete test list

TABLE B.1: Complete test list

Test number	Description	Number of fans
110	Hand-held force controller test	0
210	Software velocity test	1
211	Software velocity test	1
212	Software velocity test	1
213	Software velocity test	1
214	Software velocity test	1
300	Repeatability test 25.05	1
310	Repeatability test 26.05	1
320	Repeatability test 01.06	1
330	Repeatability test 02.06	1
331	Repeatability test 02.06	1
340	Repeatability test 07.06	1
400	Fan arm test F_x Odrive 0	1
401	Fan arm test F_x Odrive 0	1
402	Fan arm test F_x Odrive 0	1
410	Fan arm test F_x Odrive 1	1
411	Fan arm test F_x Odrive 1	1
420	Fan arm test F_x Odrive 2	1
421	Fan arm test F_x Odrive 2	1
430	Fan arm test F_y Odrive 0	1
440	Fan arm test F_y Odrive 1	1
450	Fan arm test F_y Odrive 2	1
460	Fan arm test F_z Odrive 0	1
470	Fan arm test F_z Odrive 1	1
480	Fan arm test F_z Odrive 2	1

500	Fan arm test fixed rps 0°	1
501	Fan arm test fixed rps 0°	1
502	Fan arm test fixed rps 0°	1
503	Fan arm test fixed rps 0°	1
510	Fan arm test fixed rps 45°	1
511	Fan arm test fixed rps 45°	1
512	Fan arm test fixed rps 45°	1
513	Fan arm test fixed rps 45°	1
520	Fan arm test fixed rps 67.5°	1
521	Fan arm test fixed rps 67.5°	1
522	Fan arm test fixed rps 67.5°	1
530	Fan arm test fixed rps 90°	1
531	Fan arm test fixed rps 90°	1
532	Fan arm test fixed rps 90°	1
600	Hammer test	0
600	Static load test, parallel configuration	2
610	Static load test, opposite configuration	2
700	Interaction test, static rotor, 22.5° behind	2
710	Interaction test, static rotor, 45° behind	2
720	Interaction test, static rotor, 67.5° behind	2
730	Interaction test, static rotor, 22.5° in front	2
740	Interaction test, static rotor, 45° in front	2
750	Interaction test, static rotor, 67.5° in front	2
800	Interaction test, varying rps	2
801	Interaction test, varying rps	2
802	Interaction test, varying rps	2
900	Interaction test, dynamic rotor, 22.5° angle	2
910	Interaction test, dynamic rotor, 45° angle	2
911	Interaction test, dynamic rotor, 45° angle	2
920	Interaction test, dynamic rotor, 67.5° angle	2
921	Interaction test, dynamic rotor, 67.5° angle	2
1000	Interaction test, static rotor, 22.5° behind, 30° to the side	2
1010	Interaction test, static rotor, 22.5° behind, 60° to the side	2
1020	Interaction test, static rotor, 30° behind, 22.5° to the side	2
1100	Interaction test, dynamic rotor, 22.5° behind, 30° to the side	2

1110	Interaction test, dynamic rotor, 22.5° behind, 60° to the side	2
1120	Interaction test, dynamic rotor, 30° behind, 22.5° to the side	2
1200	Perpendicular interaction test, 45° angle	2
1210	Perpendicular interaction test, 45° behind, 30° to the side	2
1211	Perpendicular interaction test, 45° behind, 30° to the side	2
1212	Perpendicular interaction test, 45° behind, 30° to the side	2
1220	Perpendicular interaction test, 67.5° angle	2
1230	Perpendicular interaction test, 67.5° behind, 30° to the side	2
1240	Perpendicular interaction test, 90° angle	2
1241	Perpendicular interaction test, 90° angle	2

Appendix C

Raw data

All raw data have been added in the electronic attachments. An example of raw data and configuration was provided of the repeatability test in Appendix C.1.

C.1 Raw data for the repeatability test

C.1.1 Configuration of the repeatability test

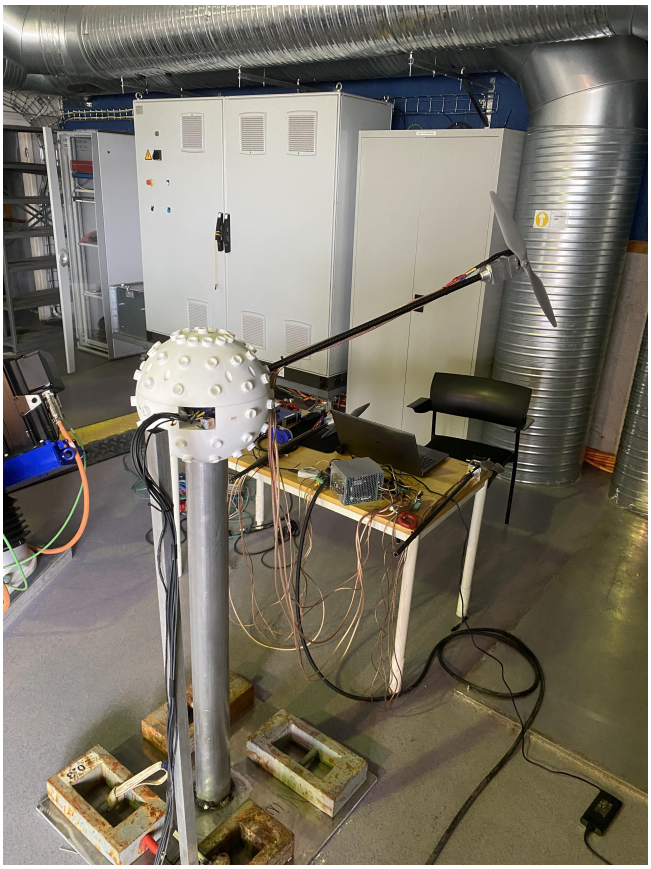

FIGURE C.1: The configuration for the repeatability test

C.1.2 Raw force data in Plotme for the repeatability test

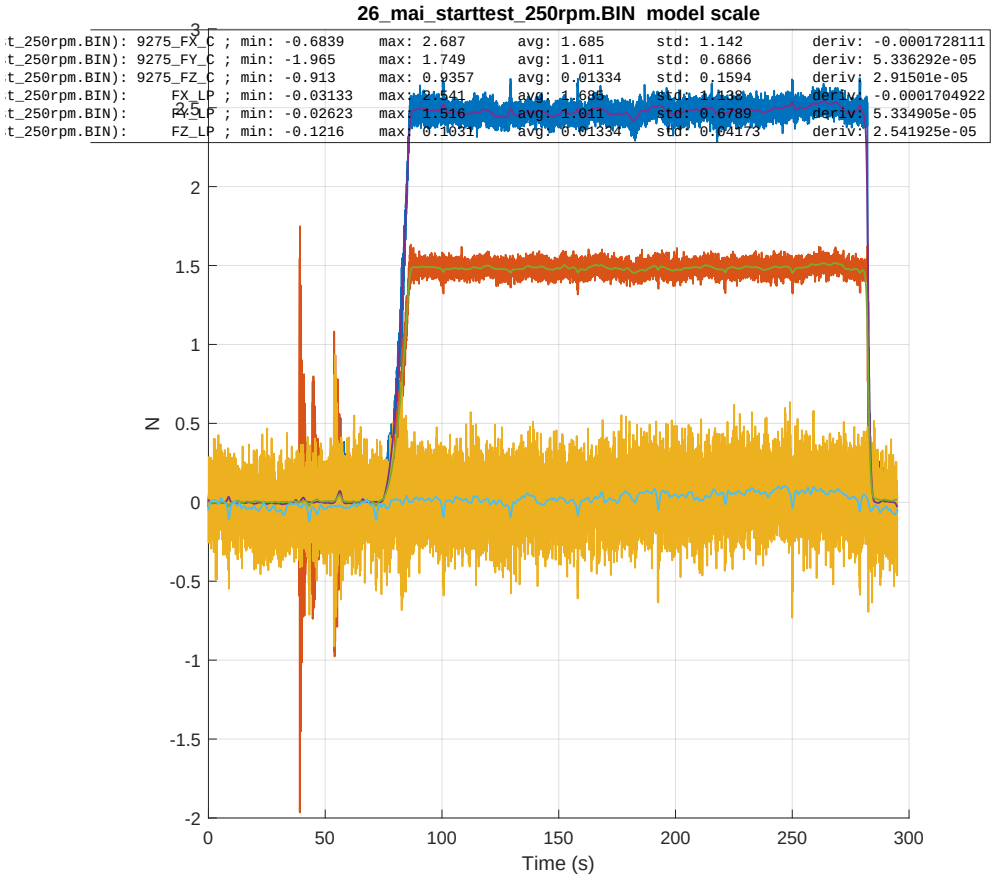

FIGURE C.2: Raw data for forces for the repeatability test

C.1.3 Raw moment data in Plotme for the repeatability test

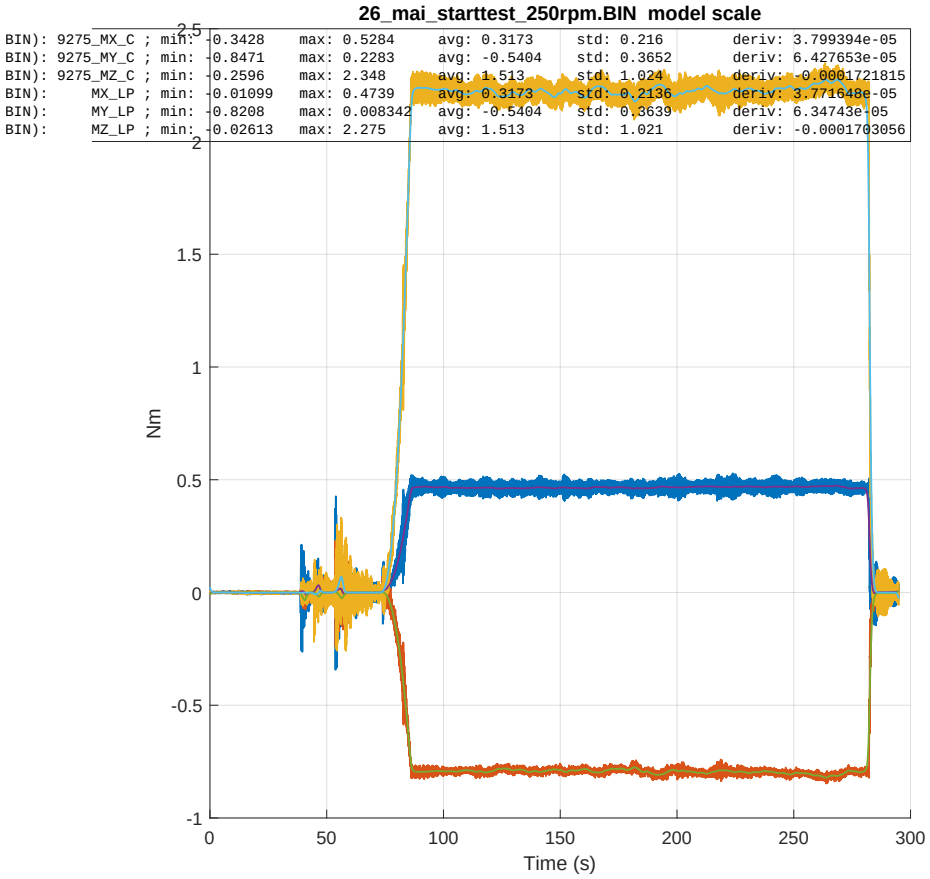

FIGURE C.3: Raw data for moments for the repeatability test

Bibliography

[1] Erlend Mørch Grova. *Actuation of loads by using fans, and application to hydrodynamic testing*. NTNU Project report, TMR4510 - Marine Control Systems, Specialization Project. Dec. 2022.

[2] Thomas Sauder et al. "Real-Time Hybrid Model Testing of a Braceless Semi-Submersible Wind Turbine: Part I — The Hybrid Approach". In: (June 2016). DOI: 10.1115/omae2016-54435.

[3] Eilif Pedersen and Hallvard Engja. *Mathematical Modelling and Simulation of Physical Systems*. Lecture Notes in TMR4275. Aug. 2014.

[4] Koichi Takanashi et al. "Non-linear earthquake response analysis of structures by a computer-actuator on-line system : Part 1 Detail of the System". In: *Transactions of the Architectural Institute of Japan* 229.0 (1975), pp. 77–83, 190. DOI: 10.3130/aijsaxx.229.0_77.

[5] Thomas Sauder. *Main concepts in cyber-physical testing*. Lecture PowerPoint, TMR18 - Cyber-physical testing in marine technology. Sept. 2022.

[6] Zoran Filipi et al. "Engine-in-the-Loop Testing for Evaluating Hybrid Propulsion Concepts and Transient Emissions - HMMWV Case Study". In: (Apr. 2006). DOI: 10.4271/2006-01-0443.

[7] A. R. Plummer. "Model-in-the-Loop Testing". In: *Proceedings of the Institution of Mechanical Engineers, Part I: Journal of Systems and Control Engineering* 220.3 (May 2006), pp. 183–199. DOI: 10.1243/09596518jsce207.

[8] Catherine A. Whyte et al. "Validation of openfresco-based thermomechanical hybrid simulation to address an earthquake-fire coupled problem". In: *COUPLED VI : proceedings of the VI International Conference on Computational Methods for Coupled Problems in Science and Engineering*. CIMNE, 2015, pp. 290–299. ISBN: 978-84-943928-3-2. URL: http://hdl.handle.net/2117/191137.

[9] Giuseppe Abbiati. *Cyber-physical testing: beyond marine technology*. Lecture PowerPoint, TMR18 - Cyber-physical testing in marine technology. Nov. 2022.

[10] Thomas Sauder. *Cable-driven parallel robots*. Lecture PowerPoint, TMR18 - Cyber-physical testing in marine technology. Oct. 2022.

[11] José Azcona et al. "Aerodynamic Thrust Modelling in Wave Tank Tests of Offshore Floating Wind Turbines Using a Ducted Fan". In: *Journal of Physics: Conference Series* 524 (June 2014), p. 012089. DOI: 10.1088/1742-6596/524/1/012089.

[12] Tommaso Battistella et al. "High Fidelity Simulation of Multi-MW Rotor Aerodynamics by Using a Multifan". In: (June 2018). DOI: 10.1115/omae2018-77606.

[13] Einar Ueland, Thomas Sauder, and Roger Skjetne. "Optimal Force Allocation for Overconstrained Cable-Driven Parallel Robots: Continuously Differentiable Solutions With Assessment of Computational Efficiency". In: *IEEE Transactions on Robotics* 37.2 (Apr. 2021), pp. 659–666. DOI: 10.1109/tro.2020.3020747. URL: https://doi.org/10.1109/tro.2020.3020747.

[14] Maxime Thys et al. "Real-Time Hybrid Model Testing of a Semi-Submersible 10MW Floating Wind Turbine and Advances in the Test Method". In: (Nov. 2018). DOI: 10.1115/iowtc2018-1081.

[15] Maxime Thys. *Cyber-physical testing of floating wind turbines*. Lecture PowerPoint, TMR18 - Cyber-physical testing in marine technology. Sept. 2022.

[16] Thomas Sauder and Sverre A. Alterskjær. "Hydrodynamic testing of wind-assisted cargo ships using a cyber–physical method". In: *Ocean Engineering* 243 (Jan. 2022), p. 110206. DOI: 10.1016/j.oceaneng.2021.110206.

[17] Alessandro Fontanella et al. "Numerical and Experimental Wind Tunnel Analysis of Aerodynamic Effects on a Semi-Submersible Floating Wind Turbine Response". In: (June 2019). DOI: 10.1115/omae2019-95976.

[18] I. Bayati et al. "A wind tunnel/HIL setup for integrated tests of Floating Offshore Wind Turbines". In: *Journal of Physics: Conference Series* 1037 (June 2018), p. 052025. DOI: 10.1088/1742-6596/1037/5/052025.

[19] Aldert Otter et al. "A review of modelling techniques for floating offshore wind turbines". In: *Wind Energy* 25.5 (Dec. 2021), pp. 831–857. DOI: 10.1002/we.2701.

[20] Vincent Arnal et al. "Hybrid Model Testing of Floating Wind Turbines: Test Bench for System Identification and Performance Assessment". In: (June 2019). DOI: 10.1115/omae2019-96374.

[21] Alessandro Fontanella et al. "A 6-DOFs Hardware-in-the-Loop System for Wind Tunnel Tests of Floating Offshore Wind Turbines". In: (June 2019). DOI: 10.1115/omae2019-95967.

[22] C Wright et al. "Experimental Comparison of Dynamic Responses of a Tension Moored Floating Wind Turbine Platform with and without Spring Dampers". In: *Journal of Physics: Conference Series* 628 (July 2015), p. 012056. DOI: 10.1088/1742-6596/628/1/012056.

[23] Felipe Vittori et al. "Model tests of a 10 MW semi-submersible floating wind turbine under waves and wind using hybrid method to integrate the rotor thrust and moments". In: *Wind Energy Science* 7.5 (Oct. 2022), pp. 2149–2161. DOI: 10.5194/wes-7-2149-2022.

[24] Mohamad Hmedi et al. "Experimental Analysis of CENTEC-TLP Self-Stable Platform with a 10 MW Turbine". In: *Journal of Marine Science and Engineering* 10.12 (Dec. 2022), p. 1910. DOI: 10.3390/jmse10121910.

[25] Cian Desmond, Jan-Christoph Hinrichs, and Jimmy Murphy. "Uncertainty in the Physical Testing of Floating Wind Energy Platforms' Accuracy versus Precision". In: *Energies* 12.3 (Jan. 2019), p. 435. DOI: 10.3390/en12030435.

[26] A Otter, J Murphy, and C J Desmond. "Emulating aerodynamic forces and moments for hybrid testing of floating wind turbine models". In: *Journal of Physics: Conference Series* 1618.3 (Sept. 2020), p. 032022. DOI: 10.1088/1742-6596/1618/3/032022.

[27] Evan Gaertner et al. *Definition of the IEA 15-Megawatt Offshore Reference Wind Turbine*. Tech. rep. International Energy Agency, 2020. URL: https://www.nrel.gov/docs/fy20osti/75698.pdf.

[28] Einar Ueland, Thomas Sauder, and Roger Skjetne. "Force Tracking Using Actuated Winches With Position-Controlled Motors for Use in Hydrodynamical Model Testing". In: *IEEE Access* 9 (2021), pp. 77938–77953. DOI: 10.1109/access.2021.3083539.

[29] Thomas Sauder. "Empirical estimation of low-frequency nonlinear hydrodynamic loads on moored structures". In: *Applied Ocean Research* 117 (Dec. 2021), p. 102895. DOI: 10.1016/j.apor.2021.102895.

[30] U. S. Department of energy. *Fans for Cooling*. URL: https://www.energy.gov/energysaver/fans-cooling (visited on 12/15/2022).

[31] Symétrie. *HEXASYM SIMULATOR*. URL: https://symetrie.fr/en/hexapods-en/software/hexasym-simulator/ (visited on 06/21/2023).

[32] Trond Innset. *15grader-vertikalt-horisontalt-01.jpg*. Email. Dec. 2022.

[33] Trond Innset. *15grader-vertikalt-horisontalt-02.jpg*. Email. Dec. 2022.

[34] Trond Innset. *kule-vindmølle-Ø300.jpg*. Email. May 2023.

[35] Trond Innset. *stang-kule-03.jpg*. Email. May 2023.

[36] Trond Innset. *vifte-03.jpg*. Email. May 2023.

[37] Trond Innset. *stang-nederst-01.jpg*. Email. May 2023.

[38] Odrive Robotics. *Odrive Motor Guide*. URL: https://docs.google.com/spreadsheets/d/12vzz7XVEK6YNIOqH0jAz51F5VUpc-lJEs3mmkWP1H4Y/edit#gid=0 (visited on 12/13/2022).

[39] APC Propellers. *16×5.5MR*. URL: https://www.apcprop.com/product/16x5-5mr/ (visited on 12/13/2022).

[40] APC Propellers. *APC Propeller Static Thrust VS. RPM Predictions*. URL: https://www.apcprop.com/files/PER2_STATIC-2.DAT (visited on 12/13/2022).

[41] Elefun.no. *Karbonrør vevd 3K - 16x14x1000mm - Bronto*. URL: https://www.elefun.no/p/prod.aspx?v=32416 (visited on 12/13/2022).

[42] Odrive Robotics. *DUAL SHAFT MOTOR - D5065 270KV - Odrive Europe*. URL: https://eu.odriverobotics.com/shop/odrive-custom-motor-d5065 (visited on 12/13/2022).

[43] Megaflis. *Skjøtekabel h07rn-f 5x2.5 16amp 400v 416-6 25m*. URL: https://www.megaflis.no/elektro/skjoteledninger/skjotekabel-h07rn-f-5x2.5-16amp-400v-416-6-25m?gclid=Cj0KCQjw8e-gBhD0ARIsAJiDsaUaAulYFNHzI

vVz6gb1mMYti9uJmXgmFo0x05ndFaGzaKT52CB4aAh8MEALw_wcB (visited on 04/15/2023).

[44] HBM. *MCS10Multicomponent sensor*. URL: https://www.hbm.com/fileadmin/mediapool/hbmdoc/technical/B04439.pdf (visited on 06/21/2023).

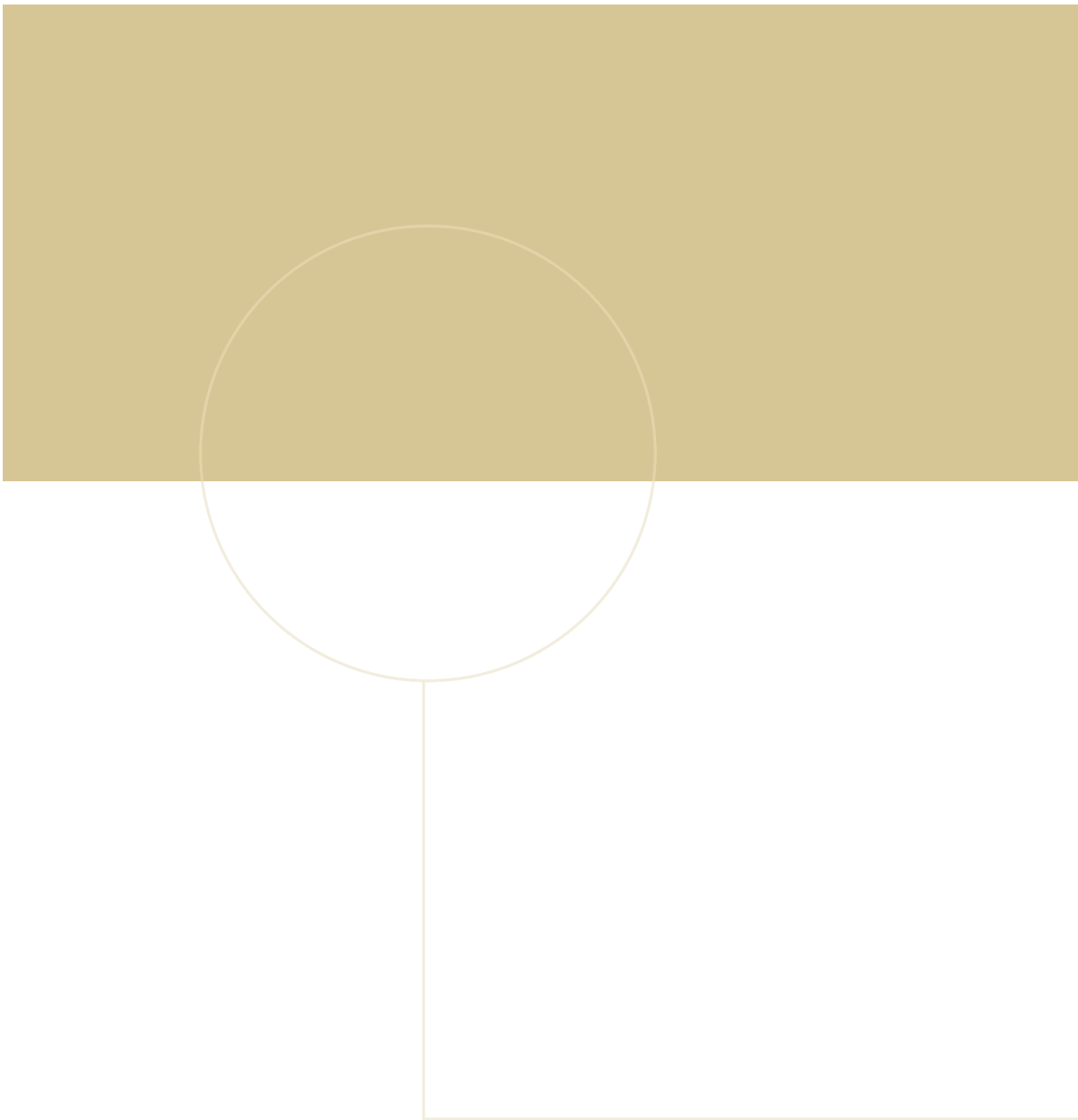

NTNU

Norwegian University of
Science and Technology